⌘ *Author's Choice*

Quantitative Proteomic Analysis of A549 Cells Infected with Human Respiratory Syncytial Virus*[S]

Diane C. Munday‡, Edward Emmott‡§, Rebecca Surtees‡, Charles-Hugues Lardeau§, Weining Wu‡, W. Paul Duprex¶, Brian K. Dove‖, John N. Barr‡§, and Julian A. Hiscox‡§‡‡**

Human respiratory syncytial virus (HRSV) is a major cause of pediatric lower respiratory tract disease to which there is no vaccine or efficacious chemotherapeutic strategy. Although RNA synthesis and virus assembly occur in the cytoplasm, HRSV is known to induce nuclear responses in the host cell as replication alters global gene expression. Quantitative proteomics was used to take an unbiased overview of the protein changes in transformed human alveolar basal epithelial cells infected with HRSV. Underpinning this was the use of stable isotope labeling with amino acids in cell culture coupled to LC-MS/MS, which allowed the direct and simultaneous identification and quantification of both cellular and viral proteins. To reduce sample complexity and increase data return on potential protein localization, cells were fractionated into nuclear and cytoplasmic extracts. This resulted in the identification of 1,140 cellular proteins and six viral proteins. The proteomics data were analyzed using Ingenuity Pathways Analysis to identify defined canonical pathways and functional groupings. Selected data were validated using Western blot, direct and indirect immunofluorescence confocal microscopy, and functional assays. The study served to validate and expand upon known HRSV-host cell interactions, including those associated with the antiviral response and alterations in subnuclear structures such as the nucleolus and ND10 (promyelocytic leukemia bodies). In addition, novel changes were observed in mitochondrial proteins and functions, cell cycle regulatory molecules, nuclear pore complex proteins and nucleocytoplasmic trafficking proteins. These data shed light into how the cell is potentially altered to create conditions more favorable for infection. Additionally, the study highlights the application and advantage of stable isotope labeling with amino acids in cell culture coupled to LC-MS/MS for the analysis of virus-host interactions. ***Molecular & Cellular Proteomics 9: 2438–2459, 2010.***

Human respiratory syncytial virus (HRSV)[1] is an enveloped RNA virus and a member of the Paramyxoviridae family, which includes common respiratory viruses such as those causing mumps and measles. HRSV is a leading cause of serious lower respiratory tract infections in infants and young children (1) and causes repeated infections throughout life. The severity of illness varies from bronchiolitis and pneumonia to common coldlike symptoms. Particular individuals at higher risk of disease include preterm infants, the immunocompromised, and elderly patients. One of the pathologies of the disease is an innate inflammatory response to infection in the lung, which could explain possible links between HRSV and asthma (2, 3). The pathogenesis of HRSV is not well understood, and to date, the development of a vaccine has been unsuccessful (4). Understanding the interaction for HRSV in particular, and for other viruses in general, with the host cell proteome, will aid in the design of effective antivirals and the development of possible vaccine strategies (5).

Because of their similar genome organization and gene expression strategy, the paramyxoviruses have been grouped

From the ‡Institute of Molecular and Cellular Biology, Faculty of Biological Sciences and §Astbury Centre for Structural Molecular Biology, University of Leeds, Leeds LS2 9JT, United Kingdom, ¶Centre for Infection and Immunity, School of Medicine and Dentistry and Biomedical Sciences, The Queen's University of Belfast, Belfast BT9 7BL, United Kingdom, and ‖Centre for Emergency Preparedness and Response, Health Protection Agency, Porton Down SP4 0JG, United Kingdom

[S] This article contains supplemental Figs. 1–3 and Tables 1–8.

⌘ *Author's Choice*—Final version full access.

Received, June 9, 2010, and in revised form, July 14, 2010

Published, MCP Papers in Press, July 20, 2010, DOI 10.1074/mcp.M110.001859

[1] The abbreviations used are: HRSV, human respiratory syncytial virus; 2DE, two-dimensional gel electrophoresis; Cdc2, cell division control protein 2 homolog; F, fusion; G, glyco; HCV, hepatitis C virus; IPA, Ingenuity Pathways Analysis; ISG15, IFN-stimulated gene 15 protein; L, large; M, matrix; m.o.i., multiplicity of infection; MSK1, mitogen- and stress-related kinase 1; N, nucleo; ND10, nuclear domain 10 structure; NDUFB, NADH dehydrogenase 1β subcomplex subunit; NF-κB, nuclear factor κB; NS, non-structural protein; nup, nucleoporin; P, phospho; PEP, posterior error probability; PHB, prohibitin; PML, promyelocytic leukemia; ROS, reactive oxygen species; SH, small hydrophobic; SILAC, stable isotope labeling with amino acids in cell culture; TOM, translocase of the outer mitochondrial membrane; VDAC, voltage-dependent anion channel; Bis-Tris, 2-[bis(2-hydroxyethyl)amino]-2-(hydroxymethyl)propane-1,3-diol; AM, acetoxymethyl ester; ECFP, enhanced cyan fluorescent protein; ES, electrospray, LQT, linear quadrupole trap.

into the Mononegavirales order that includes rabies and Ebola viruses (6). HRSV has a cytoplasmic replication strategy, and the genome consists of a single-stranded negative sense RNA with the gene order 3′ to 5′: non-structural protein 1 (NS1), non-structural protein 2 (NS2), nucleo- (N) protein, phospho- (P) protein, matrix (M) protein, small hydrophobic (SH) protein, glyco- (G) protein, fusion (F) protein, M2-1 and M2-2, and the large (L) protein. The viral proteins can be grouped into different functional categories. Four proteins are present in the viral envelope: the G, F, M, and SH proteins. The G protein plays a role in virus attachment (7), and the F protein promotes virus penetration and fusion of infected cells (8). The M protein is present in the inner viral membrane, is involved in virion morphogenesis, and traffics between the cytoplasm and the nucleus (9). The SH protein is important to viral infectivity and is a potential viroporin (10). Five proteins are involved in RNA synthesis and formation of the ribonucleocapsid structure: N and P proteins, M2-1, M2-2, and the L protein (11–14). The L protein is the catalytic component of the replicase-transcriptase complex and possesses RNA-dependent RNA polymerase activity. NS1 and NS2 are accessory proteins involved in modulating the host response to infection by acting as antagonists of the α/β interferon (IFN)-mediated antiviral state (15–17).

During infection, the virus has multiple effects on the host cell. These include (but are not limited to) cell cycle arrest through the up-regulation of transforming growth factor β1 (18), alterations in the composition of lipid raft membranes (19), decreases in members of the IFN pathways such as TRAF3 (TNF receptor-associated factor 3) and STAT2 (signal transducers and activators of transcription protein 2) (20), activation of the NF-κB signal transduction pathway (21, 22), and the activation of innate immunity through Toll-like receptor 2 (23). Many of these processes are regulated by the induction of different gene subsets (24). The relative level of host cell proteins can have a direct effect on HRSV disease progression where secondary bacterial infections are observed. For example, aberrant expression of a mucosal β-defensin leads to bacterial colonization by *Haemophilus influenzae* in HRSV infection (25).

A number of selected cellular pathways have been shown to change in HRSV-infected cells in culture and *in vivo*. Proteomics has been applied in several instances to the study of the interaction between HRSV and the host cell nuclear proteome (26). In this study, nuclear extracts from uninfected and infected cells were analyzed using two-dimensional gel electrophoresis (2DE) coupled to MALDI-TOF MS. 24 proteins whose abundance altered by $\pm$2-fold were identified and included heat shock proteins, oxidant-antioxidant enzymes, and proteins associated with nuclear domain 10 structures (ND10), which are also known as promyelocytic leukemia (PML) bodies (26). More recently, 2DE was used to compare the potential effect of several different negative strand RNA viruses, including HRSV, parainfluenza virus, human metapneumovirus, measles virus, and influenza virus, on the host cell proteome with common changes in proteins involved with apoptosis and endoplasmic reticulum stress being highlighted (27).

To take an unbiased, global approach to investigating changes in the host cell proteome in response to HRSV infection, stable isotope labeling with amino acids in cell culture (SILAC) was used in conjunction with LC-MS/MS. Through this method, cellular and possibly viral proteins were identified and quantified. To reduce sample complexity and to study the interaction of HRSV with different regions of the cell, nuclear and cytoplasmic fractions were purified and analyzed. A549 cells, a human lung carcinoma cell line that has properties similar to those of alveolar cells (which are permissive for HRSV), were used in this study. Because of its respiratory origin, this cell line has been used extensively in the characterization of HRSV infection (18, 21, 24, 28–30) and in the proteomic analysis of cellular and infectious respiratory diseases (26, 31–33). The quantitative proteomic analysis was validated using alternative techniques such as Western blot, confocal microscopy, and functional assays where appropriate. The data generated in this study indicated that there were cellular proteome alterations in HRSV-infected cells when compared with mock-infected cells and that many alterations were specific to defined protein subsets, pathways, and organelles. These included mitochondrial proteins, cell cycle regulatory proteins, ND10s, components of the nuclear pore complex, and nucleocytoplasmic trafficking proteins.

EXPERIMENTAL PROCEDURES

Cells and Virus—Hep2 and A549 cells were obtained from the Health Protection Agency Culture Collections and grown at 37 °C with 5% CO_2 in Dulbecco's modified Eagle's medium (DMEM) (Invitrogen). All cells were tested to ensure there was no contamination with mycoplasma. The media were supplemented with 10% fetal bovine serum and 1% penicillin-streptomycin. For the SILAC experiment, A549 cells were cultured in DMEM containing either ^{13}C-labeled arginine and ^{2}D-labeled lysine (R6K4-Medium) or ^{13}C- and ^{15}N-labeled arginine and lysine (R10K8-Heavy) for a minimum of seven population doublings. Labeled media were obtained from Dundee Cell Products Ltd. and were supplemented with 10% dialyzed FCS and 1% penicillin-streptomycin. Mock-infected supernatant was prepared using R6K4-Medium-labeled Hep2 cells. The HRSV A2 strain was propagated in R10K8-Heavy-labeled Hep2 cells. Virus was harvested 4 days postinfection and passed through a 0.45-μm filter. Virus titer was calculated for A549 cells using an antibody-based methylcellulose plaque assay technique based on previous studies (34, 35). Plaques were visualized using a goat anti-HRSV primary antibody (ab20745) and a horseradish peroxidase (HRP)-conjugated secondary antibody (ab6741) that were both obtained from Abcam. The latter antibody was detected using the peroxidase substrate 4-chloro-1-naphthol (Pierce). A549 cells were then grown in 500-cm^2 dishes until 60% confluent and mock-infected/infected with virus at a multiplicity of infection (m.o.i.) of 1.

Enrichment of Cytoplasmic and Nuclear Proteins by Subcellular Fractionation—Cell pellets were resuspended in a cold cytoplasmic lysis buffer (20 mM Tris-HCl, pH 7.5, 100 mM NaCl, 0.5 mM EDTA, 0.5% Nonidet P-40, EDTA-free Complete protease inhibitor mixture (Roche Applied Science)) and incubated for 10 min on ice. The su-

pernatant containing predominantly cytoplasmic proteins was collected after a 3-min centrifugation at 2,000 × *g* at 4 °C. The remaining pellet was resuspended in radioimmune precipitation assay buffer (50 mM Tris, pH 7.5,150 mM NaCl, 1% Nonidet P-40, 0.5% sodium deoxycholate, 0.1% SDS, EDTA-free Complete protease inhibitor mixture (Roche Applied Science)) and incubated for 30 min at 4 °C. The supernatant containing predominantly total nuclear protein was collected after a 2-min centrifugation at 13,000 × *g* at 4 °C. Both fractions were incubated for 5 min at 4 °C in a sonicating water bath.

Gel Electrophoresis and In-gel Digestion—Each sample was reduced in SDS-PAGE loading buffer containing 10 mM DTT and alkylated in 50 mM iodoacetamide prior to being boiled, then separated by one-dimensional SDS-PAGE (4–12% Bis-Tris Novex minigel, Invitrogen), and visualized by colloidal Coomassie staining (Novex, Invitrogen). The entire protein gel lane was excised and cut into 10 gel slices each. Gel slices were subjected to in-gel digestion with trypsin (36). The resulting tryptic peptides were extracted by 1% formic acid, acetonitrile; lyophilized in a SpeedVac (Helena Biosciences); and resuspended in 1% formic acid.

LC-MS/MS—LC-MS/MS analysis was performed by Dundee Cell Products Ltd. as described previously (37) and for completeness is reproduced here. Trypsin-digested peptides were separated using an Ultimate U3000 (Dionex Corp.) nanoflow LC system consisting of a solvent degasser, micro- and nanoflow pumps, flow control module, UV detector, and a thermostated autosampler. 10 μl of sample (a total of 2 μg) was loaded with a constant flow of 20 μl/min onto a PepMap C_{18} trap column (0.3-mm inner diameter × 5 mm; Dionex Corp.). After trap enrichment, peptides were eluted off onto a PepMap C_{18} nanocolumn (75 μm × 15 cm; Dionex Corp.) with a linear gradient of 5–35% solvent B (90% acetonitrile with 0.1% formic acid) over 65 min with a constant flow of 300 nl/min. The HPLC system was coupled to an Linear quadrupole trap Orbitrap XL (Thermo Fisher Scientific Inc.) via a nanoelectrospray ion source (Proxeon Biosystems). The spray voltage was set to 1.2 kV, and the temperature of the heated capillary was set to 200 °C. Full-scan MS survey spectra (*m/z* 335–1800) in profile mode were acquired in the Orbitrap with a resolution of 60,000 after accumulation of 500,000 ions. The five most intense peptide ions from the preview scan in the Orbitrap were fragmented by collision-induced dissociation (normalized collision energy, 35%; activation Q, 0.250; and activation time, 30 ms) in the LTQ after the accumulation of 10,000 ions. Maximal filling times were 1,000 ms for the full scans and 150 ms for the MS/MS scans. Precursor ion charge state screening was enabled, and all unassigned charge states as well as singly charged species were rejected. The dynamic exclusion list was restricted to a maximum of 500 entries with a maximum retention period of 90 s and a relative mass window of 10 ppm. The lock mass option was enabled for survey scans to improve mass accuracy (38). The data were acquired using Xcalibur software.

Quantification and Bioinformatics Analysis—Quantification was performed with MaxQuant version 1.0.7.4 (39) and was based on two-dimensional centroid of the isotope clusters within each SILAC pair. To minimize the effect of outliers, protein ratios were calculated as the median of all SILAC pair ratios that belonged to peptides contained in the protein. The percentage of variability of the quantitation was defined as the standard deviation of the natural logarithm of all ratios used for obtaining the protein ratio multiplied by a constant factor of 100.

The generation of the peak list, SILAC- and extracted ion current-based quantitation, calculated posterior error probability and false discovery rate based on search engine results, peptide to protein group assembly, and data filtration and presentation were carried out using MaxQuant. The derived peak list was searched with the Mascot search engine (version 2.1.04; Matrix Science, London, UK) against a concatenated database combining 80,412 proteins from the International Protein Index human protein database version 3.6 (forward database) and the reversed sequences of all proteins (reverse database). Alternatively, database searches were done using Mascot (Matrix Science) as the database search engine, and the results were saved as a peptide summary before quantification using MSQuant (http://msquant.sourceforge.net/). Parameters allowed included up to three missed cleavages and two labeled amino acids (arginine and lysine). Initial mass deviation of the precursor and fragment ions were up to 7 ppm and 0.5 Da, respectively. The minimum required peptide length was set to six amino acids. To pass statistical evaluation, posterior error probability (PEP) for peptide identification (MS/MS spectra) should be below or equal to 0.1. The required false positive rate was set to 5% at the peptide level. False positive rates or PEPs for peptides were calculated by recording the Mascot score and peptide sequence length-dependent histograms of forward and reverse hits separately and then using Bayes' theorem in deriving the probability of a false identification for a given top scoring peptide. At the protein level, the false discovery rate was calculated as the product of the PEP of the peptides of a protein where only peptides with distinct sequences were taken into account. If a group of identified peptide sequences belongs to multiple proteins and these proteins cannot be distinguished with no unique peptide reported, these proteins are reported as a protein group in MaxQuant. Proteins were quantified if at least one MaxQuant-quantifiable SILAC pair was present. Identification was set to a false discovery rate of 1% with a minimum of two quantifiable peptides. The set value for false positive rate/PEP at the peptide level ensures that the worst identified peptide has a probability of 0.05 of being false, and proteins are sorted by the product of the false positive rates of their peptides where only peptides with distinct sequences are recognized. During the search, proteins are successively included starting with the best identified proteins until a false discovery rate of 1% is reached, an estimation based on the fraction of reverse protein hits. Enzyme specificity was set to trypsin allowing for cleavage N-terminal to proline and between aspartic acid and proline. Carbamidomethylation of cysteine was searched as a fixed modification; *N*-acetyl protein and oxidation of methionine were searched as variable modifications.

Data sets of identified and both identified and quantified cellular and viral proteins in the nuclear and cytoplasmic fractions are presented in supplemental Tables 1–7. Here, information is included such as the protein identification in the International Protein Index format, the abundance as a ratio of HRSV/mock, the UniProt identification, number of peptides used to identify the protein, the sequence coverage this represents, predicted protein details such as molecular weight and length, the gel slice in which this protein was present, and the PEP score. Note that for the ratio of HRSV/mock a score of 0.5 or lower indicates a 2-fold or greater decrease in abundance in HRSV-infected cells and that a score of 2 or more indicates a 2-fold or greater increase in abundance in HRSV-infected cells in the appropriate fraction.

Protein Pathway Analysis—Data were analyzed through the use of Ingenuity Pathways Analysis (Ingenuity® Systems, www.ingenuity.com). Networks were generated using data sets containing gene identifiers and corresponding expression values that were uploaded into the application. Each gene identifier was mapped to its corresponding gene object in the Ingenuity Pathways Knowledge Base. A cutoff of 2.0 was set to identify genes whose expression was significantly differentially regulated. These genes, called focus genes, were overlaid onto a global molecular network developed from information contained in the Ingenuity Pathways Knowledge Base. Networks of these focus genes were then algorithmically generated based on their connectivity. Graphical representations of the molecular relationships between genes/gene products were generated. Genes or gene products are represented as nodes, and the biological relationship between two nodes is repre-

sented as an edge (line). All edges are supported by at least one reference from the literature or from canonical information stored in the Ingenuity Pathways Knowledge Base. Human, mouse, and rat orthologs of a gene are stored as separate objects in the Ingenuity Pathways Knowledge Base but are represented as a single node in the network. The intensity of the node color indicates the increased (red) or decreased (green) abundance. Nodes are displayed using various shapes that represent the functional class of the gene product. Canonical pathway analysis utilizes well characterized metabolic and cell signaling pathways that are generated prior to data input and on which identified proteins are overlaid.

Immunofluorescence—Coverslip-adhered A549 cell monolayers were infected with HRSV at an m.o.i. of 1 or 2. The plates were rocked periodically at 37 °C over a 2-h incubation period before the inoculum was replaced with fresh growth media and the plate was incubated at 37 °C for a further 24 h. The cells were fixed with formalin, and the following antibodies were applied. VDAC1 (20B12) (ab14734), prohibitin (II-14-10) (ab1836), TOMM20 (ab56783), and TOMM22 (ab57523) were obtained from Abcam. NADH dehydrogenase 1β subcomplex subunit (NDUFB) 10 (SAB1400181) and FLAG (M2) (F1804) were obtained from Sigma. Lamin B (101-B7) (NA12) was obtained from Merck, and PML (PG-M3) (sc-966) was obtained from Santa Cruz Biotechnology. Alexa Fluor-conjugated secondary antibodies (A21050, A11004, and A11061) were obtained from Molecular Probes (Invitrogen). HRSV proteins were detected by either a goat anti-HRSV primary antibody (ab20745) recognized by a FITC-conjugated secondary (ab6881) or through the use of a FITC-conjugated anti-HRSV A2-specific primary antibody (ab20391). Coverslips supporting the fixed and stained cells were mounted onto glass slides using either Vectorshield (Vector Laboratories) or Prolong Gold® antifade reagent (Invitrogen), both of which contain a DAPI counterstain to allow visualization of cell nuclei.

Confocal Microscopy—Direct and/or indirect immunofluorescence confocal microscopy images were captured on an LSM510 META microscope (Carl Zeiss Ltd.) equipped with 40× and 63×, 1.4 numerical aperture, oil immersion lenses. Pinholes were set to allow optical sections of 1 μm to be acquired. Where possible, all fluorescence was measured in the linear range as the detector is a photomultiplier, and the range indicator was utilized to ensure that no saturated pixels were obtained on image capture. However, for certain images depending on the distribution of the protein, some parts of the image were outside of the linear range to clearly show the distribution of the appropriate protein. Images were averaged either four or eight times.

Trafficking Analysis of P and M2-1 Proteins—The P and the M2-1 genes were amplified by reverse transcription-PCR from total RNA extracted from HRSV A2-infected cells. Complementary DNA served as a template for PCR amplification and was subcloned into TOPO TA vector pCR2.1 (Invitrogen). The P gene was then cloned into the cyan fluorescent vector pECFP-C1 (Clontech), and the M2-1 gene was cloned into pTri-ExNeo vector (Novagen). The orientation of the insert was confirmed by sequencing (data not shown). A549 cell monolayers were grown on glass coverslips in 12-well dishes, transfected with 2 μg/well plasmid using Lipofectamine 2000 in Opti-MEM (Invitrogen) according to the manufacturer's instructions, and added to antibiotic-free media. After 24 h at 37 °C, the transfection mixture was removed. The plates were then incubated as described above for a further 24 h. Control wells of transfection only and media only were included to assess any background reactivity. Nuclei were stained with propidium iodide (Invitrogen), and coverslips were mounted onto glass slides with glycerol.

Western Blotting—The cellular fractions were obtained as detailed above, and total protein concentration was determined by BCA assay (Pierce). Protein fractions (2 μg) were resolved by 12% SDS-PAGE and transferred to PVDF membranes (Millipore) using a Bio-Rad semi-dry transfer apparatus. Immobilized proteins were detected with the following antibodies. Tubulin (YOL1/34) (ab6161), lamin B1 (119D5-F1) (ab8982), cell division control protein 2 homolog (Cdc2) (A17) (ab18), and nucleolin (4E2) (ab13541) were obtained from Abcam. Lamin B (101B7) (NA12) was obtained from Merck, and cyclin A (H-432) (sc-751), cyclin B1 (D-11) (sc-7393), cyclin D2 (M-20) (sc-593), and cyclin E (M-20) (sc-481) were obtained from Santa Cruz Biotechnology. HRSV proteins were detected by a goat anti-HRSV primary antibody (ab20745) from Abcam. Three HRP-conjugated secondary antibodies (A5795, A4416, and A6154) were obtained from Sigma, and one (ab6741) was from Abcam; all were detected by enhanced chemiluminescence (ECL). For the PML Western blot, 10 μg of nuclear protein and 4 μg of cytoplasmic protein were resolved by 15% SDS-PAGE and transferred to a PVDF membrane as described above. Immobilized proteins were detected with PML (PG-M3) (sc-966) obtained from Santa Cruz Biotechnology. The HRP-conjugated secondary antibody (A4416) was detected using SuperSignal ECL (34095) obtained from Pierce.

Mitochondrial Transition Pore Assay and Live Cell Imaging—Glass bottom plate- and coverslip-adhered A549 cell monolayers were infected with HRSV at an m.o.i. of 2 or mock-infected. The plates were rocked periodically at 37 °C for 2 h before the inoculum was replaced with fresh growth media and the plates were incubated at 37 °C for a further 24 h. The ImageiT^{TM} LIVE Mitochondrial Transition Pore Assay kit (I35103) obtained from Molecular Probes (Invitrogen) was used (according to the manufacturer's instructions) to visualize the mitochondrial transition pore in HRSV-infected, mock-infected, and positive control cells.

PML Localization—Coverslip-adhered A549 cell monolayers in 6-well dishes were transfected with 2 μg/well FLAG-PML-I or FLAG-PML-II (40) using Lipofectamine 2000 in serum-free media according to the manufacturer's instructions. After the 2-h incubation at 37 °C, the transfection mixture was removed, and the cell monolayers were infected and incubated as described above. Control wells of transfection only and media only were included to assess any background reactivity. The cells were fixed with formalin and detected with the following antibodies. A FITC-conjugated anti-HRSV-specific primary antibody (ab20391) obtained from Abcam was used to detect HRSV proteins. Both tagged PML isoforms were detected with an anti-FLAG M2 (F1804) primary antibody that was obtained from Sigma-Aldrich. Alexa Flour-conjugated secondary antibodies (A1106 and A1104) were obtained from Molecular Probes (Invitrogen). The nuclei of the above fixed cells were stained with DAPI contained within the Vectorshield (Vector Laboratories) used to mount the coverslips onto glass slides.

RESULTS

Quantitative proteomic analysis was used to investigate the potential changes in the host cell proteome in response to infection with HRSV. Cells were fractionated into nuclear and cytoplasmic extracts to reduce sample complexity for LC-MS/MS but also to provide an excellent way to further probe the interaction of a cytoplasmic replicating virus with the nuclear and cytoplasmic proteomes. To our knowledge, no previous study has used SILAC coupled with LC-MS/MS to identify and quantify proteome changes in cells infected with HRSV or any other single-stranded negative sense RNA viruses. The observed changes were then validated and investigated using a combination of immunofluorescence to study subcellular localization, Western blot to study protein abundance, and functional assays applied where appropriate.

Identification and Quantification of Cellular and Viral Proteins—Labeled A549 cells were infected with HRSV at an m.o.i. of 1 or mock-infected with supernatant that was prepared in the same way as described for the labeled virus stock. Labeling, validation, fractionation, protein identification, and quantification were conducted as outlined in Fig. 1. Mock-infected cells were grown in media labeled with R6K4-Medium, and cells infected with virus were grown in media containing R10K8-Heavy. Proteins were identified and quantified at 24 h postinfection. Indirect immunofluorescence confocal microscopy indicated that 60–70% of cells treated with HRSV were infected (Fig. 1*B*). Fluorescence was not detected in mock-infected cells (Fig. 1*B*). Cells were enriched into cytoplasmic and nuclear fractions, which were validated by the detection of characteristic cellular (tubulin for the cytoplasm and lamin B1 for the nucleus) (Fig. 1*C*) and viral (Fig. 1*D*) marker proteins that were enriched in the respective fractions. The protein concentration was determined by BCA assay. Note that equal protein concentrations were loaded, and therefore quantitative comparison of the relative abundance of proteins between the cytoplasmic and nuclear fractions should not be made. Western blot analysis showed that there was no virus present in mock-infected cells (Fig. 1*D*).

LC-MS/MS analysis identified 606 and 534 proteins in the nuclear (supplemental Table 1) and cytoplasmic (supplemental Table 2) fractions, respectively. Of these, 561 and 520 proteins were identified and quantified in the nuclear and cytoplasmic fractions, respectively. All proteins were identified by two or more peptides. Mitochondrial proteins (74 proteins; supplemental Table 3) were present in the nuclear fraction, and these were removed from the final list of proteins assigned to the nuclear proteome (supplemental Table 4). The proteins classified as forming the cytoplasmic proteins are shown in supplemental Table 5. A previous analysis of nuclear fractions obtained from A549 cells (prepared by a different method) also contained mitochondrial proteins, which were shown to be contaminants (33). Five viral proteins were identified in both fractions (NS1, N, P, M, and M2-1 proteins), and one viral protein, F protein, was identified in the cytoplasmic fraction only (see supplemental Tables 6 and 7 for viral proteins found in the nuclear and cytoplasmic fractions, respectively).

For quantitative analysis, previous investigations using SILAC and LC-MS/MS have applied ratio cutoffs ranging from near 1.3- to 2.0-fold (41). A previous study that investigated changes in the nuclear proteins in HRSV-infected cells used a ratio cutoff of 2.0-fold for comparison (26). In this study, a 2.0-fold cutoff was chosen as a basis for investigating potential proteome changes between data sets through IPA and to provide a basis for comparing the current data set with previous studies. The comparison of mock-infected with HRSV-infected cells indicated that in the nuclear fraction many proteins showed a 2-fold or greater decrease in abundance (supplemental Table 1), whereas in the cytoplasmic fraction, very few proteins changed in abundance (supplemental Table 2).

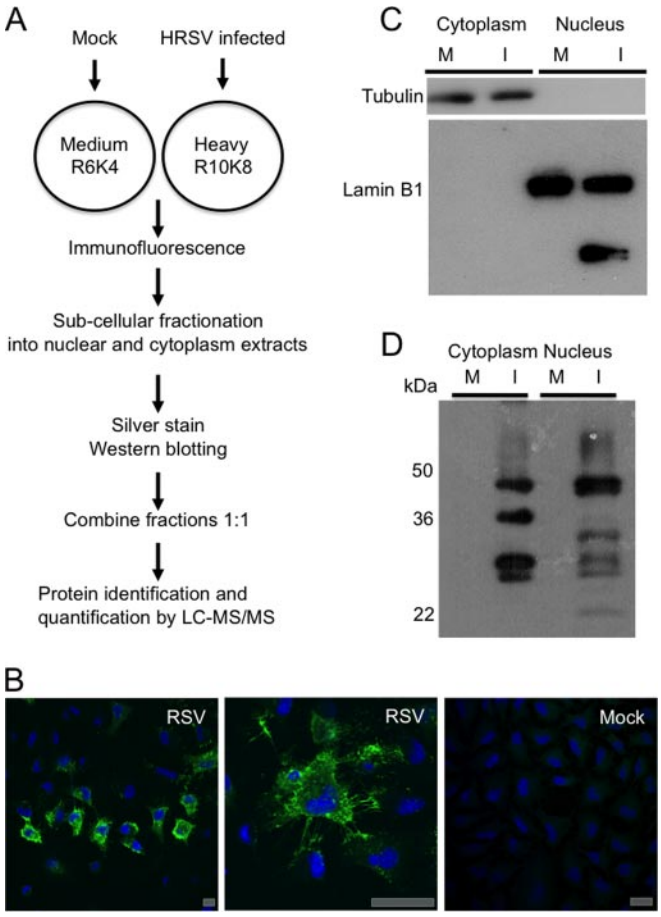

FIG. 1. **Quantitative proteomics using SILAC of HRSV-infected cells *versus* mock-infected cells.** *A*, a diagrammatic representation of the methodology used in this analysis. Stable isotope (medium and heavy)-labeled amino acids were incorporated into newly synthesized cellular proteins. A549 cells were infected with HRSV (heavy) alongside a mock infection (medium), and 24 h postinfection subcellular fractionation was used to enrich the cytoplasmic and nuclear proteins. The infection efficiency and the fraction purity were then validated prior to sample preparation and LC-MS/MS analysis. *B*, indirect immunofluorescence confocal microscopy validation of HRSV infection efficiency in A549 cells 24 h postinfection. Staining with the HRSV antibody combination in mock-infected cells is shown as a control. Different magnifications are presented. *Scale bars*, 20 μm. *C*, Western blot confirmation of representative proteins enriched from the cytoplasmic and the nuclear fractions of mock-infected (*M*) and HRSV-infected (*I*) cells. Membrane-immobilized proteins were detected with tubulin (~55 kDa) and lamin B1 (~58 kDa) antibodies. Tubulin and lamin B1 were predominately localized in the cytoplasmic and nuclear fractions, respectively. *D*, Western blot confirmation of HRSV infection (and lack thereof in mock-infected cells). An anti-HRSV-specific polyclonal primary antibody was detected by an HRP conjugate. The locations of molecular mass markers (kDa) are indicated on the *left*, and the tentative assignments of proteins are indicated on the *right*. *RSV*, respiratory syncytial virus.

Bioinformatics Analysis of Nuclear and Cytoplasmic Fractions in A549 Cells—The nuclear proteome for A549 cells, corresponding to 433 genes, has been resolved previously (33). In the current study, the nuclear and cytoplasmic pro-

teomes were resolved to study the interaction of HRSV with the host cell. IPA was used to assign identified proteins into different molecular and cellular functional classes (see supplemental Table 8 for definitions) based upon the underlying biological evidence from the curated Ingenuity Pathways Analysis literature database. The relative proportions of proteins represented in each separate functional class in the nuclear and cytoplasmic proteomes of A549 cells are shown in Fig. 2. The data indicated that the proteomes differed between the nuclear and cytoplasmic fractions. As would be expected, a greater proportion of proteins involved in gene expression, post-transcriptional modification of RNA, and RNA trafficking were present in the nuclear fraction than in the cytoplasmic fraction, and a greater proportion of proteins involved in protein degradation and lipid metabolism were present in the cytoplasmic fraction than in the nuclear fraction.

Pathway analysis was used to group proteins into different functional networks to determine whether different cellular activities were altered in HRSV-infected cells. For example, in the nuclear fraction, proteins involved in cell growth and transcription regulation (Fig. 3) were less abundant in HRSV-infected cells. Such pathways were linked by cell cycle regulatory complexes (*e.g.* cyclin A) and IFN β, which were not identified in the LC-MS/MS analysis. Additionally, in the nuclear fraction, proteins involved in molecular transport and protein and RNA trafficking could be grouped together, and all were less abundant in the nucleus in HRSV-infected cells (Fig. 4). In the cytoplasmic fraction, proteins involved in cellular assembly and organization, cellular compromise, and protein folding were grouped together. Proteins could be linked by NF-κB and STAT1 signaling for example (Fig. 5).

Several canonical pathways were highlighted by Ingenuity Pathways Analysis as being disrupted in HRSV-infected cells, including those involved in mitochondrial dysfunction (39 of a possible 172 molecules; p value, 5.89×10^{-29}), ubiquinone biosynthesis (15 of 119 molecules; p value, 6.69×10^{-29}), and RAN signaling (six of a possible 23 molecules; p value, 1.87×10^{-6}). Other identified cellular proteins altered in HRSV-infected cells included components of subnuclear structures such as the nucleolus (nucleolin and nucleophosmin) and ND10s (*e.g.* TAR DNA protein), the latter of which had been previously highlighted as changing in HRSV-infected cells (33), and cell cycle regulatory molecules. A number of proteins that were ablated could be grouped into specific disease associations, including respiratory disease (22 proteins; p values, 6.84×10^{-4}–2.59×10^{-2}), the inflammatory response (12 proteins; p values, 5.59×10^{-4}–4.56×10^{-2}), and infectious disease (73 proteins; p values, 5.81×10^{-10}–2.59×10^{-2}). For example, six proteins were associated with pneumonitis, which can be a feature of HRSV infection (42).

Selected results of the IPA were validated using alternative techniques. These included Western blot, indirect and direct immunofluorescence confocal microscopy, and functional assays from biological replicates. Confocal microscopy, unlike Western blot, does not rely on subcellular fractionation and purification of proteins from mock- or HRSV-infected cells and thus provides complete, independent verification of the results. This information was combined with an examination of the previously existing literature to form the basis of validation for the quantitative proteomics analysis and to further investigate the findings.

Validation of IPA Analysis for HRSV-infected Cells Using Previously Characterized Immune Signaling—The HRSV-immune response interaction has been well characterized *in vitro* and *in vivo* (*e.g.* Ref. 20). In the quantitative proteomics analysis of A549 cells infected with HRSV, STAT1 and its downstream molecule IFN-stimulated gene 15 protein (ISG15) were more abundant than in mock-infected cells (Fig. 5, *left*). This observation reflects previous work in which human diploid fibroblast 2fTGH cells were infected with HRSV, and STAT1 protein was shown to be more abundant in HRSV-infected cells when compared with mock-infected cells (43). The role of STAT1 in the immunobiology of HRSV has been investigated in transgenic animal models (44). The IFN-stimulated gene 15 mRNA and protein were shown to be upregulated in a mouse lung epithelial cell line (MLE-15) infected with HRSV (45). In the current data set, these molecules were linked to NF-κB-activated transcription, transforming growth factor β1, and IFN α/β (Fig. 5), all of which have been described in HRSV-infected cells (5, 18, 20, 21, 44, 46, 47). Therefore, previously published data were reflected by the bioinformatics analysis of the current quantitative proteomics data.

Alterations in Mitochondrial Protein Abundance and Mitochondrial Integrity in HRSV-infected Cells—As highlighted by the canonical pathway analysis, mitochondrial proteins formed a group whose abundance differed between HRSV-infected and mock-infected cells. This had not been observed previously. Mitochondrial proteins were identified and quantified in both the nuclear and cytoplasmic fractions as being both ablated and enriched proteins in HRSV-infected cells compared with mock-infected cells (supplemental Tables 1–3). This is presented diagrammatically in Fig. 6 with the proteins arranged according to their localization in the mitochondria.

Respiratory Complex 1 proteins and other mitochondrial proteins identified and quantified by LC-MS/MS (Fig. 6) were decreased in abundance by 2-fold or more in HRSV-infected cells in comparison with mock-infected cells. For example, respiratory Complex 1 protein NDUFB10 was 60-fold decreased in the nuclear fraction but not represented in the cytoplasmic fraction. The abundance of the translocase of the outer mitochondrial membrane (TOM) complex subunits Tom20, Tom22, Tom40, and Tom70 were decreased ~129-, 26-, 15-, and 12-fold, respectively, in the nuclear fraction enriched from HRSV-infected cells but were not detected in

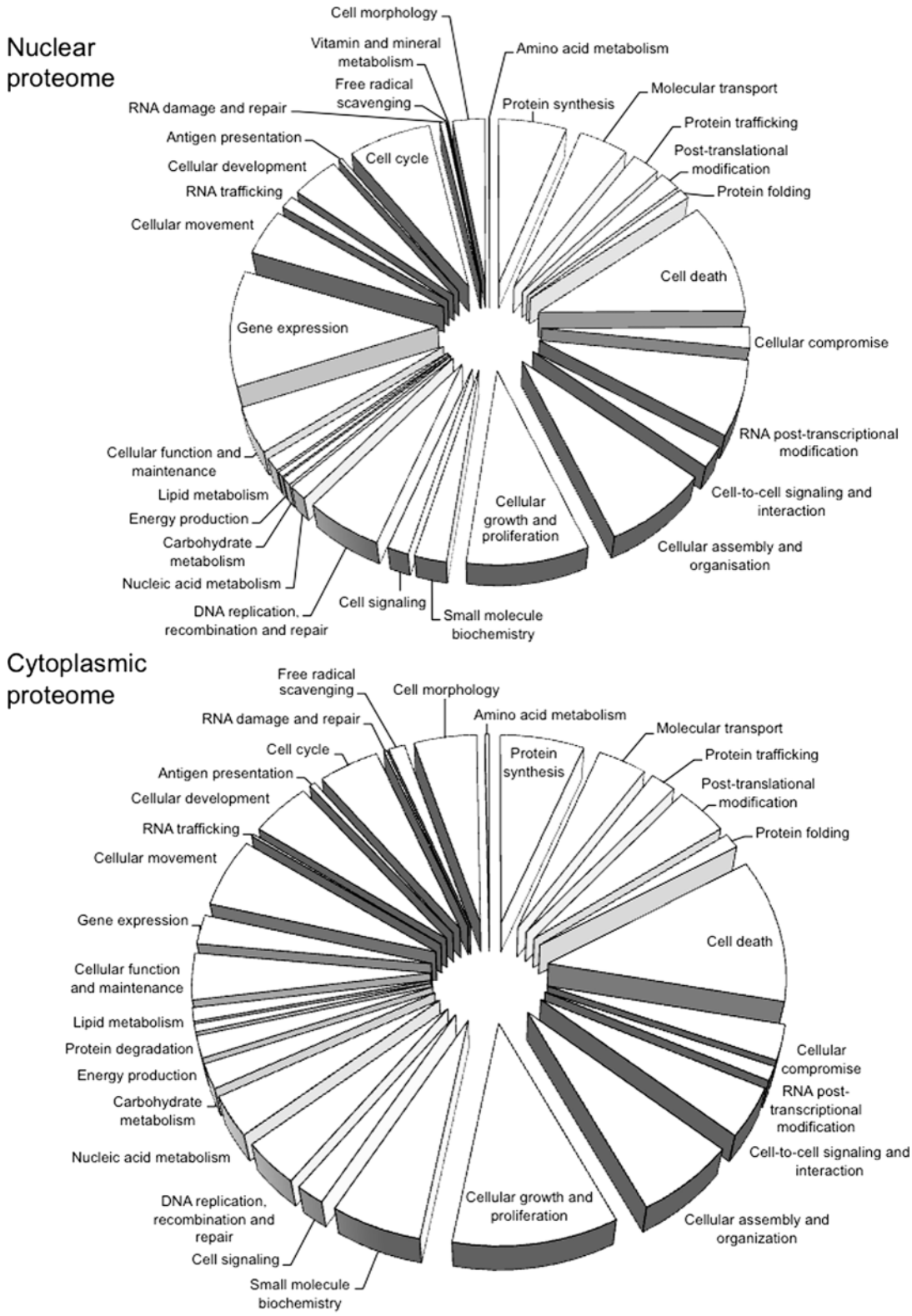

FIG. 2. **Classification of cellular proteins in HRSV-infected A549 cells according to their assigned fraction and biological function.** For orientation, proteins classified as being involved in protein synthesis are to the *right* of the *12 o'clock position* followed *clockwise* by protein synthesis, RNA post-transcriptional modification, cellular growth and proliferation, protein degradation (cytoplasmic fraction only), gene expression, and RNA trafficking. Formal descriptions of the different assigned functions are presented in supplemental Table 8.

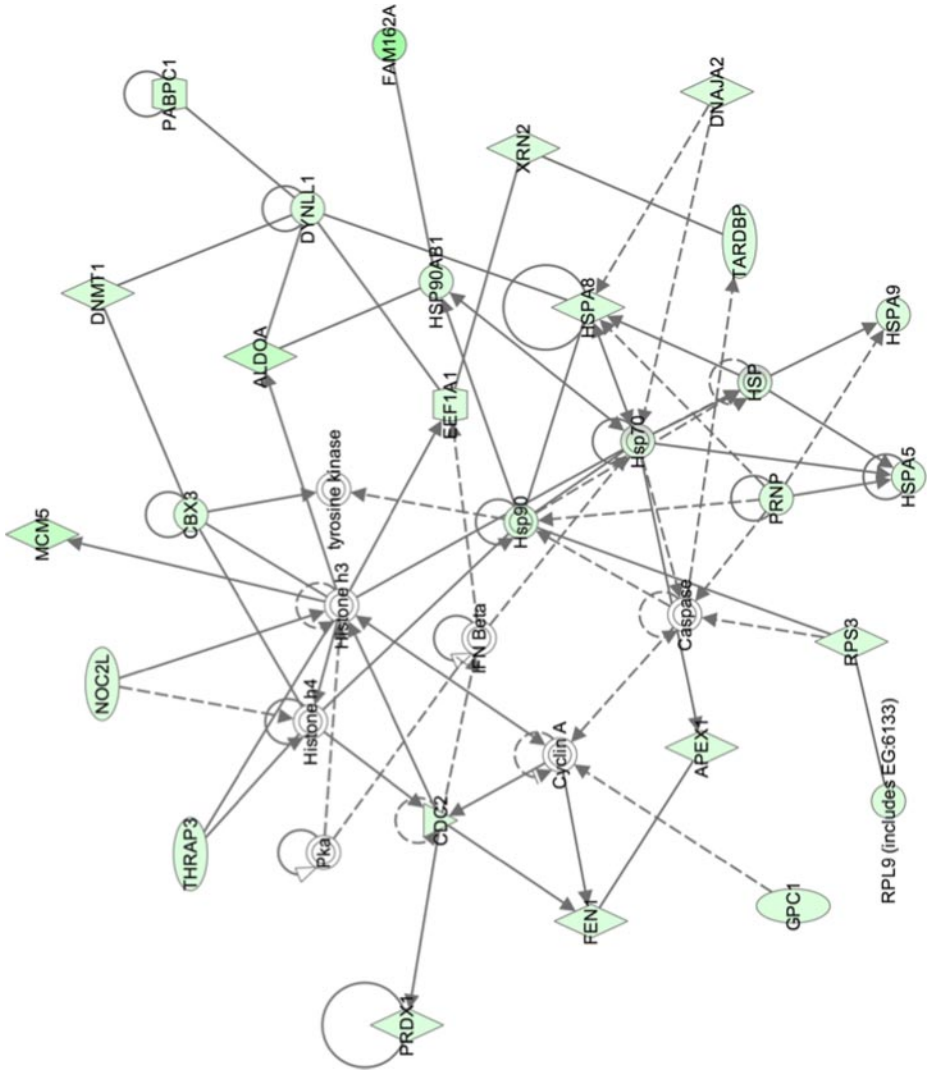

FIG. 3. **Network pathway analysis of proteins identified in nuclear fraction that are primarily involved in cell growth and transcription regulation.** Proteins shaded in *green* indicate a 2-fold or greater decrease in abundance in the nuclear fraction of HRSV-infected cells compared with mock-infected cells, and the *color intensity* corresponds to the degree of abundance. Proteins in *white* are those identified through the Ingenuity Pathways Knowledge Base. The *shapes* denote the molecular class of the protein. A *solid line* indicates a direct molecular interaction, and a *dashed line* indicates an indirect molecular interaction. A full explanation of lines and relationships is provided in supplemental Fig. 3.

the cytoplasmic fraction. The abundance of voltage-dependent anion channel (VDAC) proteins 1, 2, and 3 were decreased by ~31-, 42-, and 26-fold, respectively, in the nuclear fraction in HRSV-infected cells compared with mock-infected cells. VDAC1 and VDAC2 were also detected in the cytoplasmic fraction with 10- and 9-fold increases, respectively, in HRSV-infected cells when compared with mock-infected cells. Prohibitin (PHB) subunits PHB1 and PHB2, which are involved in cell proliferation and the functional integrity of mitochondria (48, 49), were increased 3-fold in the cytoplasmic fraction from HRSV-infected cells.

Indirect immunofluorescence confocal microscopy was used to investigate the localization and possible abundance of the mitochondrial proteins in HRSV-infected cells. The NDUFB10 localization validation indicated that the subcellular localization of this protein was altered in HRSV-infected cells when compared with mock-infected cells, and increased fluorescence intensity was also observed in the former (Fig. 7*A*). The fluorescence data for the subcellular localization of representative TOM complex members (Tom20 and Tom22) indicated that the subcellular localization of these proteins also differed between HRSV-infected cells and mock-infected cells with localization observed in a distinct region of the cytoplasm. There also appeared to be less fluorescence from Tom20 and Tom22 in HRSV-infected cells (Fig. 7, *B* and *C*, respectively). In addition, the data indicated that in HRSV-infected cells Tom20 was possibly present in the nucleus or at least closely associated with this structure. This was confirmed in the Z-stack image of this cell (supplemental Fig. 1). The relative fluorescence of VDAC1 in HRSV-infected cells was greater than in mock-infected cells. The subcellular localization was also altered with increased punctate staining observed (Fig. 8*A*). The subcellular localization of PHB in HRSV-infected cells appeared to be localized with viral complexes and with greater fluorescence intensity in these regions than in mock-infected cells (Fig. 8*B*).

Together, the indirect immunofluorescence confocal microscopy images supported the observations from the quan-

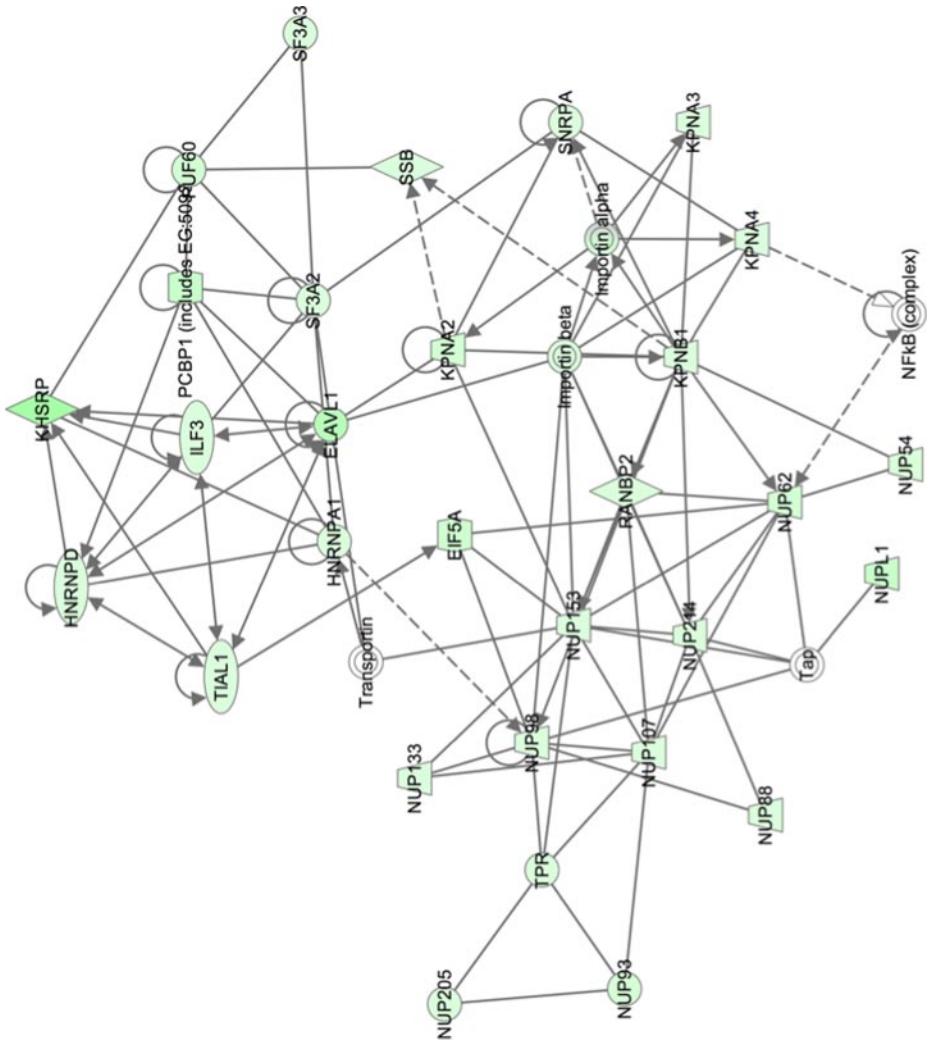

FIG. 4. **Network pathway analysis of proteins identified in nuclear fraction that are primarily involved in molecular transport, including protein and RNA trafficking.** Proteins shaded in *green* indicate a 2-fold or greater decrease in abundance in the nuclear fraction of HRSV-infected cells compared with mock-infected cells, and the *color intensity* corresponds to the degree of abundance. Proteins in *white* are those identified through the Ingenuity Pathways Knowledge Base. The *shapes* denote the molecular class of the protein. A *solid line* indicates a direct molecular interaction, and a *dashed line* indicates an indirect molecular interaction. A full explanation of lines and relationships is provided in supplemental Fig. 3.

titative proteomic analysis that the abundance of mitochondrial proteins (particularly pore proteins) was altered in HRSV-infected cells. From this, we hypothesized that the mitochondrial permeability transition pores had an altered function in HRSV-infected cells. To test this hypothesis, we made use of a live cell mitochondrial assay in which green fluorescent (calcein AM) dye is maintained in healthy mitochondria (which are also stained red with a MitoTracker dye). As a positive control, cells were treated with the Ca^{2+} ionophore ionomycin, which results in mitochondrial pore activation from the inner and outer mitochondrial membranes and subsequent loss of green fluorescence. In this live cell assay, it was not possible to use indirect immunofluorescence confocal microscopy to visualize HRSV-infected cells (as the cells could not be made permeable to allow antibody penetration). Therefore, cells were infected at an m.o.i. of 2 to ensure that at least 70% of cells were infected at 24 h postinfection, the assay point (after the experiment, cells were fixed, and infection status confirmed using indirect immunofluorescence confocal microscopy (supplemental Fig. 2)). The data illustrated that in mock-infected cells the majority of the cells were stained green and red, indicating functional mitochondria (Fig. 9). In control cells treated with ionomycin, all of the cells were stained red with no green signal, indicating mitochondrial pore activation (Fig. 9). In HRSV-infected cells, there was a greater population of predominately red cells than predominately green cells, indicating greater mitochondrial pore activation in cell populations infected with HRSV in comparison with the mock-infected cells (Fig. 9).

Potential Disruption of Proteins Involved in Nucleocytoplasmic Trafficking—Network pathway analysis indicated that the abundance of nuclear pore complex components and proteins involved in the nucleocytoplasmic trafficking of proteins and RNA differed between HRSV-infected and mock-infected cells (Fig. 4). The proteins, their position in the nuclear pore complex, and their possible associations can be seen in Fig. 10*A*. Assignment of the localization of the localization of these proteins within the nuclear pore complex was based on data from a number of different studies (50–56). Additionally, nup155 and nup107 identified in the study but not shown in

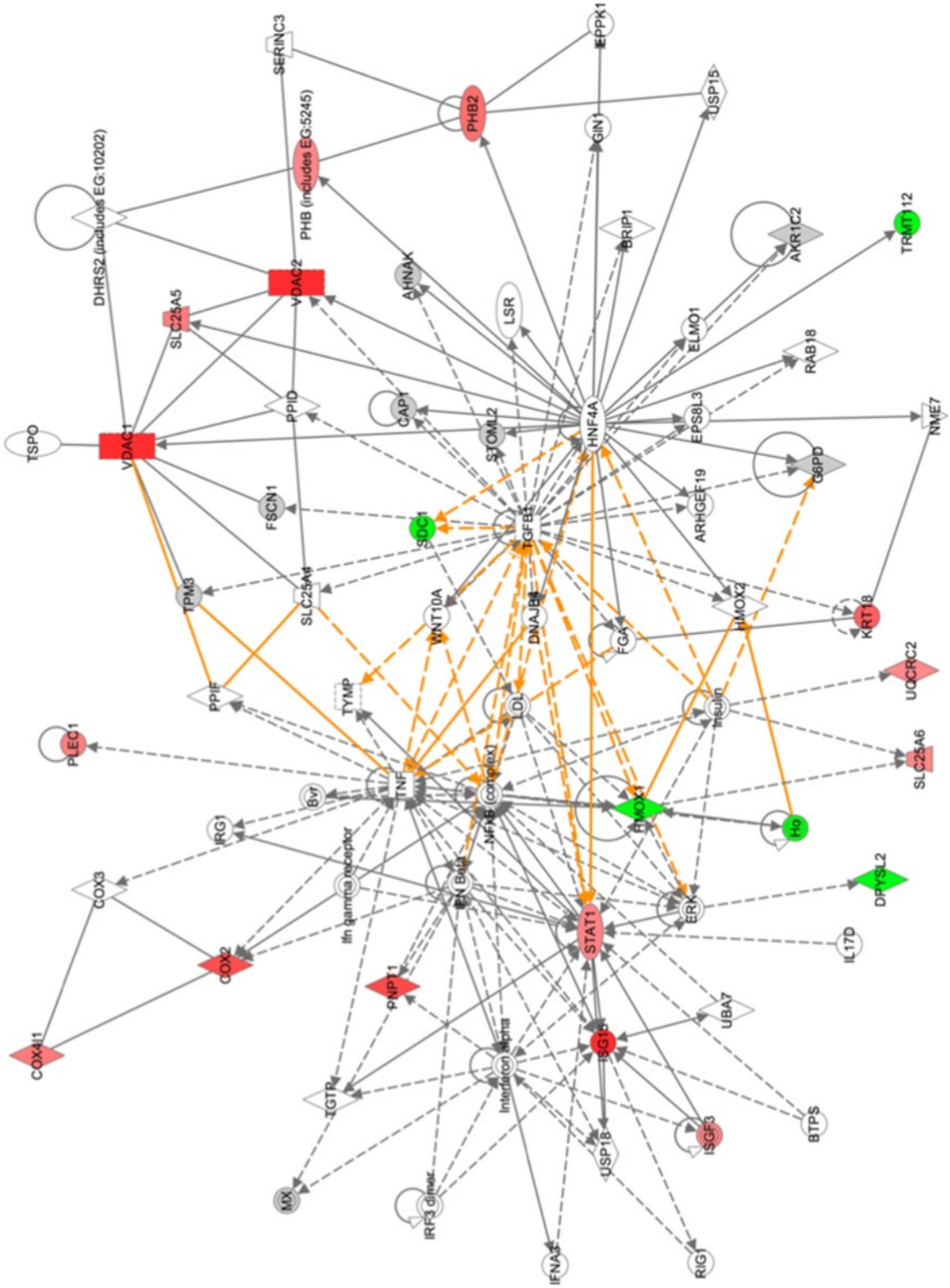

FIG. 5. **Merged network pathway analysis of proteins involved in cellular assembly and organization, cellular compromise, and protein folding that were identified in cytoplasmic fraction.** Proteins shaded in *green* indicate a 2-fold or greater decrease in abundance, and proteins shaded in *red* correspond to a 2-fold or greater increase in the cytoplasmic fraction of HRSV-infected cells. The *color intensity* denotes the degree of abundance. Proteins in *white* are those identified through the Ingenuity Pathways Knowledge Base. The *shapes* denote the molecular class of the protein. A *solid line* indicates a direct interaction, and a *dashed line* indicates an indirect interaction. The *yellow lines* denote the linkage between the pathways through NF-κB and STAT1 signaling. A full explanation of lines and relationships is provided in supplemental Fig. 3.

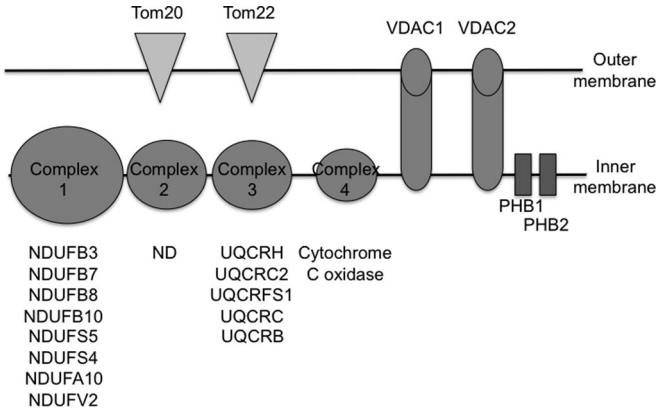

FIG. 6. **Alterations in mitochondrial protein abundance and mitochondrial integrity in HRSV-infected cells.** A diagrammatic representation shows the inner and outer mitochondrial membranes with representative proteins identified in the quantitative proteomic analysis shown in their appropriate mitochondrial localizations. In the outer mitochondrial membrane, Tom20 and Tom22 interact with other Toms (some of which were identified in this analysis) to form a pore through which premitochondrial proteins are transported. Transmembrane pores such as VDACs may participate in the formation of the permeability transition pore complex, which is responsible for the release of mitochondrial products such as cytochrome *c* that trigger apoptosis. The inner membrane contains the protein complexes involved in the electron transport chain. Respiratory Complexes 1, 3, and 4 are proton pumps. Those proteins involved in cell proliferation and integrity such as PHB subunits PHB1 and PHB2 are also found in mitochondria.

Fig. 10*A* were shown to be involved in nuclear envelope and pore complex formation (57, 58).

The quantitative proteomic analysis indicated that in HRSV-infected cells nucleoporins (nups) were depleted; *e.g.* nup96 and nup98 were depleted 3.6-fold (and those shown in Fig. 10*A*). The only exceptions were nup85 and nup160. Indirect immunofluorescence confocal microscopy was used to investigate the subcellular localization of the nuclear protein lamin B in mock-infected cells in comparison with HRSV-infected cells (Fig. 10*B*). The data indicated that in mock-infected cells the protein was localized to the nuclear envelope but also was distributed between the nucleus and the cytoplasm. In contrast, in HRSV-infected cells, lamin B appeared to be more concentrated around the nuclear envelope with less fluorescence observed in the cytoplasm or the nucleus, which is indicative of altered trafficking or loss of nuclear pore complex function.

Alteration of Cell Cycle Regulatory Proteins in HRSV-infected Cells—The quantitative proteomics and network pathway analysis (Fig. 3) identified several proteins with roles in cell cycle regulation whose abundance differed between mock-infected and HRSV-infected cells. These included Cdc2 (also known as cyclin-dependent kinase 1 (cdk1)); histone deacetylase 2 (HDAC2); proliferation-associated 2G4, 38 kDa (PA2G4); and SIN3 homolog A transcription regulator (yeast) (SIN3A) (~6-, 4-, 3-, and 3-fold less abundant, respectively, in HRSV-infected cells). Network pathway analysis (Fig. 3) also predicted that cyclin A might be altered in HRSV-infected cells. Cdc2 has been shown to bind to cyclins such as A, E, and B types and can regulate cell cycle progression (59, 60). In addition, in HRSV-infected A549 cells, cell cycle arrest has been observed; however, the abundance of cell cycle regulatory complexes was not elucidated (18). Western blot analysis of nuclear and cytoplasmic fractions from mock- and HRSV-infected cells indicated that Cdc2 was less abundant in the nuclear fraction in HRSV-infected cells (confirming the quantitative proteomic analysis) and that cyclins D2, A, E, and B1 were also less abundant (Fig. 11). In such analysis, it is essential to ensure that equal protein loading is used to allow for relative protein abundance observations. Lamin B and tubulin were therefore selected as internal controls to confirm protein content.

Disruption to Subnuclear Structures, ND10s (PML Bodies), and Associated Proteins—Many subnuclear structures such as the nucleolus and ND10s (also known as PML bodies) contain proteins that are involved in the antiviral signaling response that become altered in virus-infected cells (61–63). The nucleolus is formed from a complex of protein-protein and protein-nucleic acid interactions centered around nucleolar hub proteins such as nucleolin and nucleophosmin (64). ND10s are formed around PML protein and are dynamic structures that are in continuous protein exchange with the nucleus, depending on the metabolic state of the cell (65). PML is a protein with several different isoforms that can localize to ND10s and/or the nucleus or cytoplasm (66). Several components of the subnuclear structures were altered in HRSV-infected cells, including an ablation of nucleolin (decreased 4.5-fold) and nucleophosmin (decreased 6.7-fold) (see supplemental Table 1; for nucleolin, shown using Western blot, see Fig. 11).

The following constituents of ND10s were altered in abundance in HRSV-infected cells: the TAR DNA-binding protein (~−3-fold), eukaryotic translation initiation factor 3 (~−9-fold), and DNA repair protein RAD50 (~−2.6-fold). ND10 abundance and localization were investigated in HRSV-infected through the use of its major constituent, PML. An antibody that recognized all PML isoforms was applied to both Western blot and indirect immunofluorescence analysis. Western blot analysis indicated that more PML isoforms were present in the nuclear fraction from HRSV-infected cells when compared with mock-infected cells (Fig. 11). In the cytoplasmic fraction in HRSV-infected cells, a decreased abundance in the number of PML isoforms was observed when compared with the mock-infected cells (Fig. 11). The indirect immunofluorescence confocal microscopy data indicated that there were a greater number of ND10s present in the HRSV-infected cells when compared with mock infected-cells (Fig. 12). This observation included not only cells that were positively identified as infected but also the bystander cells (Fig. 12). This result was in contrast to a previous proteomic anal-

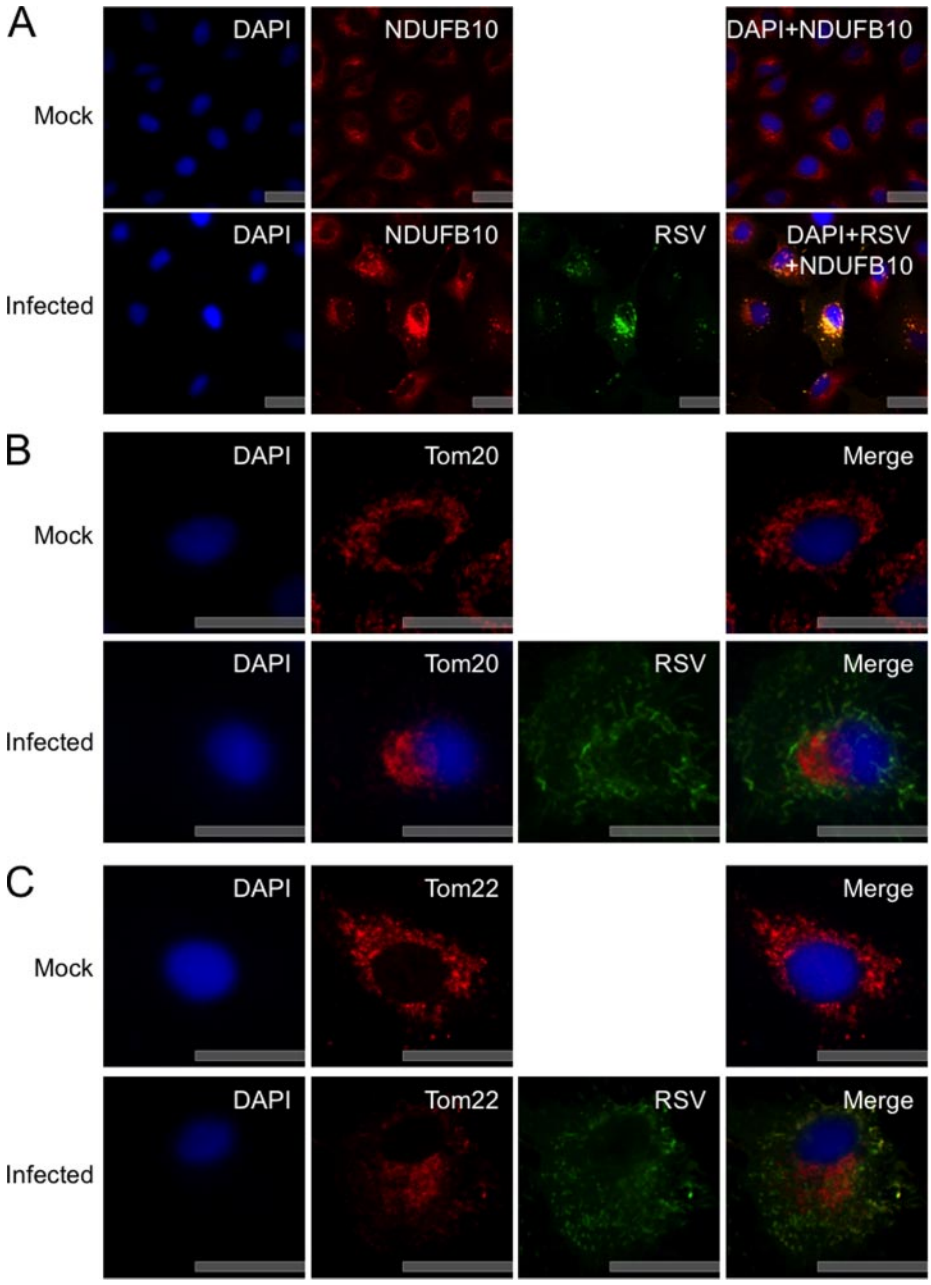

FIG. 7. ***A*, indirect immunofluorescence confocal microscopy analysis of the subcellular localization of NDUFB10 in mock- and HRSV-infected A549 cells 24 h postinfection.** NDUFB10 proteins are stained *red*, HRSV proteins are shown in *green*, and the nuclei are stained *blue* with DAPI. A merge image is also presented. *B* and *C*, indirect immunofluorescence confocal microscopy analysis of examples of outer mitochondrial membrane proteins whose abundance was shown to change in the quantitative proteomic analysis of the subcellular localization of Tom20 and Tom22 in mock- and HRSV-infected A549 cells 24 h postinfection. Tom20 (*B*) and Tom22 (*C*) proteins are stained *red*, HRSV proteins are *green*, and nuclei are stained *blue* with DAPI. A merge image is also presented. *Scale bars*, 20 μm. *RSV*, respiratory syncytial virus.

ysis of the nucleus from HRSV-infected A549 cells proposing that PML protein is redistributed from the nucleus to the cytoplasm 24 h postinfection (26). In the current study, further analysis of HRSV-infected cells at 36 h postinfection indicated that PML remained predominately in the nucleus with no change in the number of ND10s in mock-infected cells (Fig. 12). To confirm that PML was not redistributed to the cytoplasm in mock-infected and HRSV-infected cells in our experimental system, overexpression analysis of two PML isoforms, recombinant FLAG-tagged PML-I and PML-II (40), was used (Fig. 12). The data indicated that both tagged fusion proteins remained localized to the nucleus at 24 h postinfection, which was the same in mock-infected cells (Fig. 12).

Identification of Viral Proteins in Nuclear and Cytoplasmic Fractions—The LC-MS/MS analysis identified several viral proteins in the nuclear and cytoplasmic fractions (supplemental Tables 6 and 7, respectively). Although the data tables show a quantitative ratio between HRSV proteins and mock-infected cells, in reality this should be infinite and is a result of comparison with cellular peptides of similar sequence. HRSV replication is cytoplasmic, therefore, the potential presence of viral proteins in the nucleus may be considered an unusual observation. However, HRSV M protein has been shown to localize to the nucleus and contains nuclear-cytoplasmic trafficking signals (9, 67–69). The presence of viral proteins in the nuclear fraction either may have been

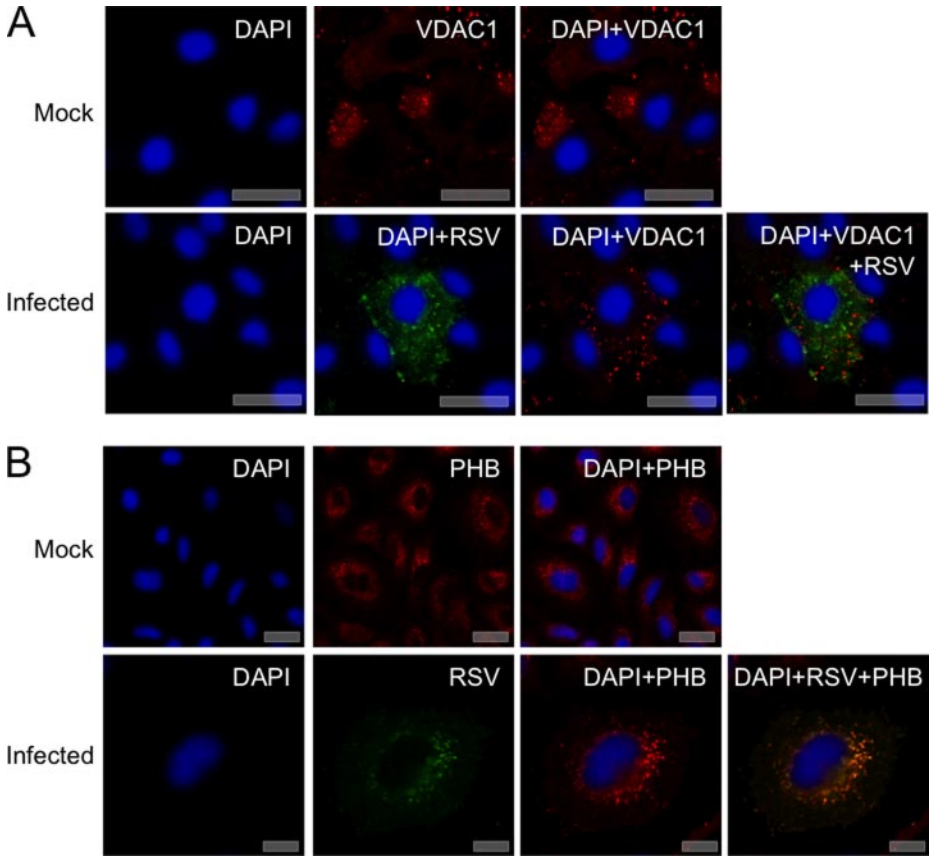

FIG. 8. **Indirect immunofluorescence confocal microscopy analysis of examples of mitochondrial transmembrane and inner membrane proteins whose abundance was shown to change in quantitative proteomic analysis of subcellular localization of VDAC1 and PHB in mock- and HRSV-infected A549 cells 24 h postinfection.** VDAC1 proteins (*A*) and PHB proteins (*B*) are stained *red*, HRSV proteins are *green*, and nuclei are stained *blue* with DAPI. A merge image is also presented. *Scale bars*, 20 μm. *RSV*, respiratory syncytial virus.

an artifact of the fractionation procedure or may reflect the subcellular localization of a protein. To investigate whether the HRSV P and M2-1 proteins were present in the nucleus, overexpression analysis was utilized where these proteins were expressed as C-terminal fluorescent fusion proteins tagged with cyan (ECFP). The direct fluorescence confocal microscopy analysis indicated that both the P and the M2-1 proteins localized predominately to the cytoplasm, but some fluorescent signal was observed in the nucleus but excluded from the nucleolus (Fig. 13). This correlates with the identification of these proteins in the nuclear fraction. ECFP was localized throughout the cell. Note that ECFP and the fusion proteins have been false colored green postimage capture for increased clarity.

DISCUSSION

HRSV infection results in multiple changes in the host cell, and the aim of this study was to provide an unbiased global overview of these effects. The quantitative proteomics and the subsequent bioinformatics analysis using IPA allowed alterations in the host cell proteome to be mapped in HRSV-infected cells. This study serves to reflect the existing *in vitro* and *in vivo* data and highlights new interactions. To our knowledge, no such SILAC-coupled LC-MS/MS study has been applied to HRSV or to any other single-stranded negative sense RNA virus. Despite the potential of this technique and transferable application to the comparison of treated with non-treated experimental conditions (41, 70), a few studies have used this methodology to investigate the interactions of viruses with the host cell. These include investigations of the interaction of hepatitis C virus (HCV) with cell lipid rafts (71), pseudorabies virus-infected cells (72), coronavirus-infected cells (37), and alterations to the nucleolar proteome in adenovirus- (73) and coronavirus (74)-infected cells.

Identification and Quantification of Cellular Proteins and Experimental Conditions—Potential changes in the host cell cytoplasmic and nuclear proteomes were elucidated for a HRSV subgroup A using optimized conditions to ensure that the majority of cells were infected with HRSV to generate the highest potential differences between the mock- and HRSV-infected cell treatments for LC-MS/MS quantification and data comparison. The laboratory-adapted HRSV A2 strain used in animal-based pathogenesis studies (75) was used in the SILAC study because it replicated to high efficiency in the A549 model cell line. These cells have been used extensively in HRSV studies because of their ability to retain features of alveolar cells (76). Proteins were identified and quantified at 24 h postinfection as this time point occurs prior to the appearance of a major cytopathic effect; thus, the majority of cells remain viable for downstream processing. In addition, this time point is commonly used in HRSV studies and there-

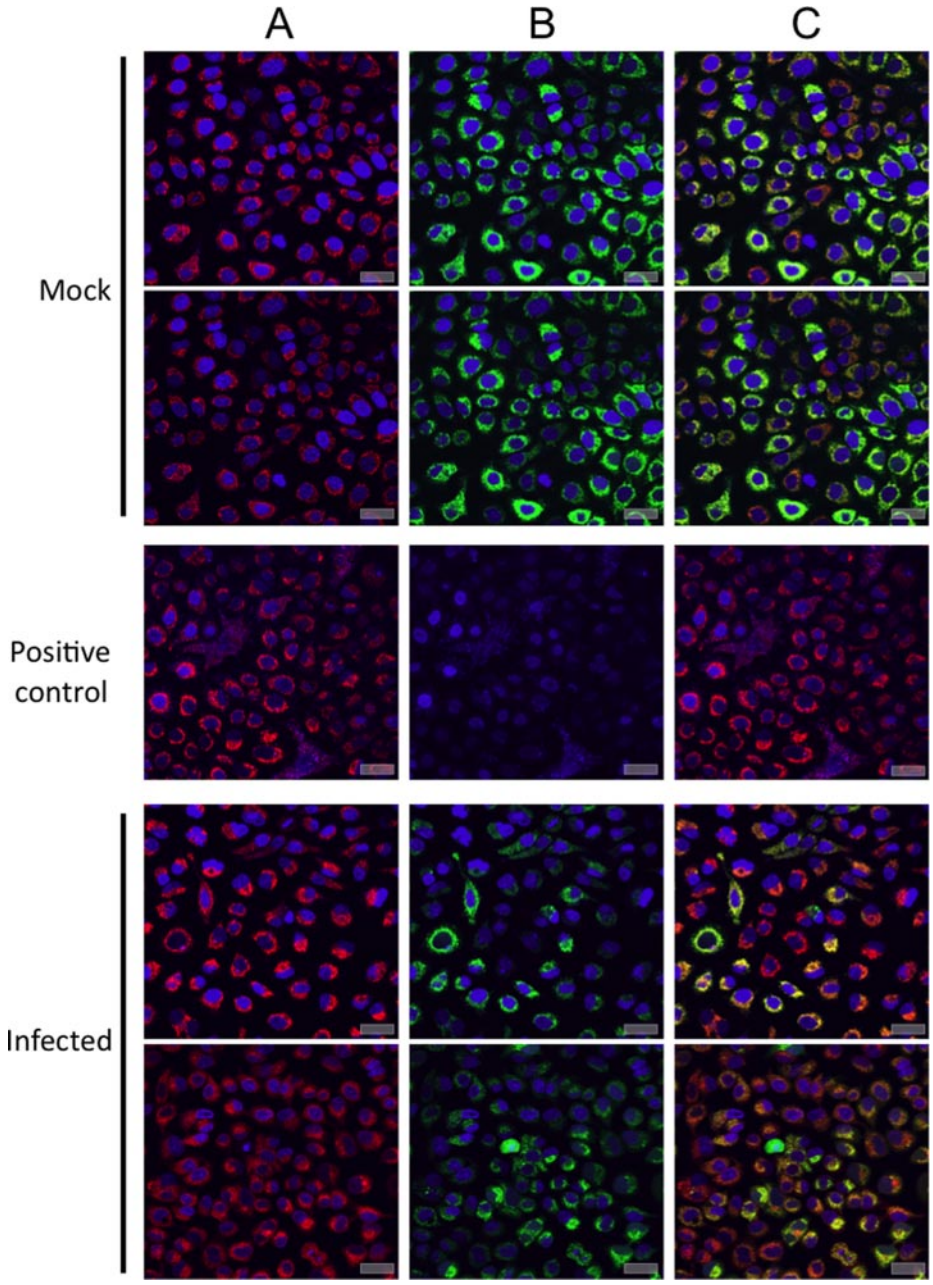

FIG. 9. **Live cell confocal microscopy analysis of mitochondrial transition pore activity in mock- and HRSV-infected A549 cells 24 h postinfection.** Nuclei are stained *blue* with Hoechst. All mitochondria are stained *red* with Mito-Tracker (*A*), healthy cells are also stained *green* with calcein AM (*B*), which is concentrated in the mitochondria. Merged images are also presented (*C*). Positive control cells were treated with ionomycin to allow the entry of excess calcium into the cells to trigger mitochondrial pore activation, which leads to the release of calcein AM and therefore the loss of green florescence. A large proportion of mitochondria in HRSV-infected cells were stained *red* and only weakly *green*, indicating that HRSV infection affected mitochondrial transition pore activity. *Scale bars*, 20 μm. Note that indirect immunofluorescence confocal microscopy was used to demonstrate that cells were infected with HRSV, and these data are presented in supplemental Fig. 2.

fore allows comparison with the previously published data. For example, microarray studies (24) of HRSV-infected cells have demonstrated a high return of data at this time point. In total, 606 cellular proteins were identified in the nuclear fraction, and 534 proteins were identified in the cytoplasmic fraction along with six viral proteins.

Curiously, of a total of 510 proteins assigned to the nuclear proteome, 431 showed a 2-fold or greater decrease in abundance in HRSV-infected cells. This could not be attributed to a preparation or loading artifact as equal protein concentrations between the mock and infected preparations were validated using independent assays such as a BCA assay and staining after separation by one-dimensional SDS-PAGE, and large volumes were combined to reduce variation in liquid handling prior to LC-MS/MS analysis. Also, nuclear proteins with increased and decreased abundances between mock and infected cells were validated experimentally using alternative techniques on the same and different samples, *e.g.* the increased abundance of PML *versus* the decreased abundance of nucleolin and similar levels of marker proteins such as lamin B (*e.g.* Figs. 1 and 11). A similar study of potential changes in the nuclear proteome in cells infected with an avian coronavirus reflected a general trend in the decreased abundance of nuclear proteins (37).

Using Ingenuity Pathways Analysis, these proteins were grouped into functional classes and used to potentially map

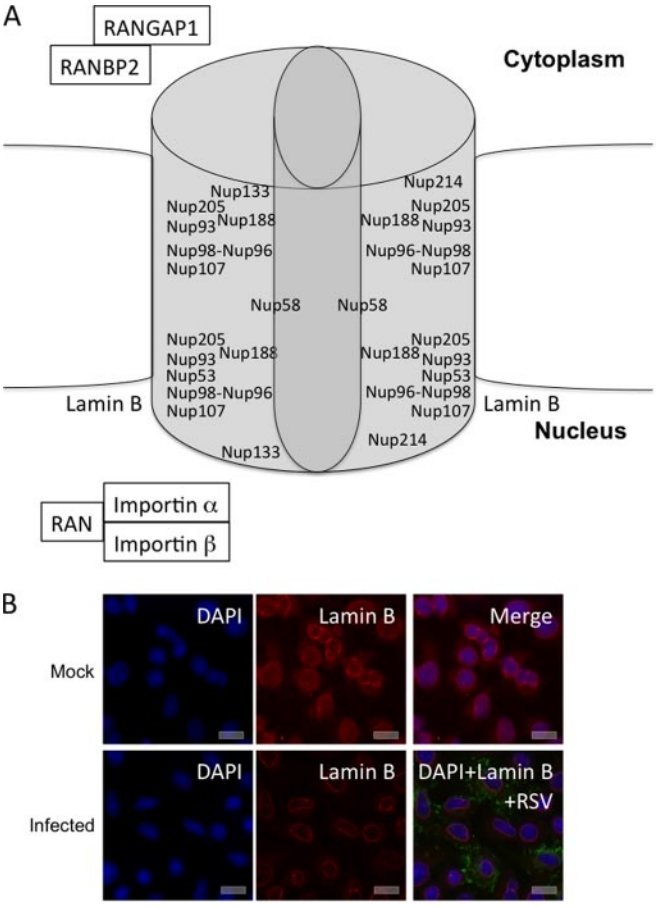

FIG. 10. **Potential disruption of proteins involved in nucleocytoplasmic trafficking in HRSV-infected cells.** *A*, a diagrammatic representation of the nuclear pore complex showing examples of the nuclear pore proteins whose abundance was altered in the quantitative proteomic analysis of HRSV-infected *versus* mock-infected cells and also nucleocytoplasmic trafficking proteins. Many of the nups interact with one another and other nuclear envelope proteins; for example, nup53 interacts with nup98 and lamin B. *B*, indirect immunofluorescence confocal microscopy analysis of nuclear protein lamin B subcellular localization in mock- and HRSV-infected A549 cells 24 h postinfection. Lamin B proteins are stained *red*, HRSV proteins are shown in *green*, and the nuclei are stained *blue* with DAPI. A merge image is also presented. *Scale bars*, 20 μm. *RSV*, respiratory syncytial virus.

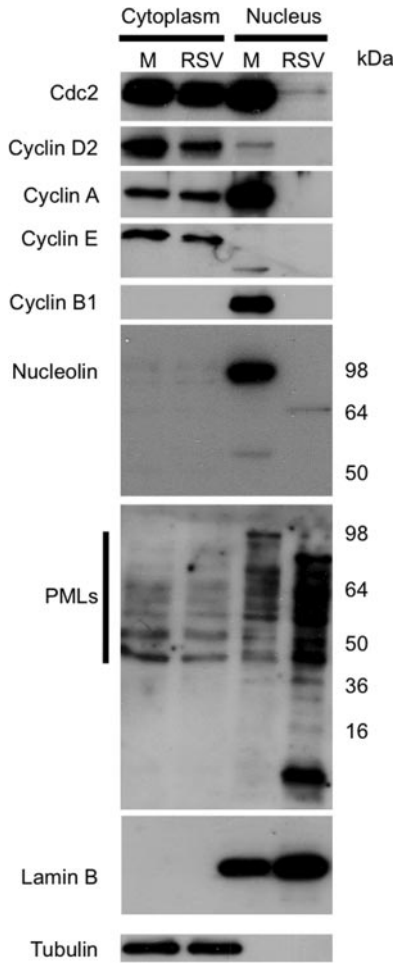

FIG. 11. *A*, Western blot analysis of the cell cycle regulatory proteins and components of subnuclear structures in HRSV-infected (*RSV*) *versus* mock-infected cells (*M*) present in cytoplasmic and nuclear fractions. To validate fraction enrichment and loading control, tubulin and lamin B were used as markers for the cytoplasm and nucleus, respectively.

the nuclear and cytoplasmic proteomes of A549 cells (Fig. 2). The nuclear proteome of A549 cells has been investigated previously using 2DE and HPLC, highlighting the extensive use of A549 cells in respiratory disease research (33). Therefore, our current study complements and expands this analysis and adds further data on cytoplasmic proteins.

Network Pathway Analysis—IPA was used to analyze the data sets, investigate potential changes in specific cellular functions, and generate a priority list of proteins and pathways of interest. IPA identified several different biological pathways, some of which may be common to viral infection. For example, in common with the data gathered for HRSV-infected A549 cells, a proteomic analysis of the $CD4^+$ CEMx174 cell line infected with HIV-1 highlighted changes in the carrier proteins in nucleocytoplasmic trafficking, cyclin-dependent kinases, and ubiquitination (77). The latter process has also been identified in proteomic analysis of cells infected with avian infectious bursal disease virus (78).

Highlighted results from the quantitative proteomics study and subsequent network pathway analysis were selected for validation and further investigation using alternative approaches. The results were compared with the previously published literature, and indirect immunofluorescence confocal microscopy, Western blot, and functional analysis techniques were also applied in independent experiments separate from the quantitative proteomic analysis.

HRSV Pathologies and Immune Signaling—In this quantitative proteomic analysis, several different proteins involved in the pathologies and the immune signaling associated with HRSV infection were altered. For example, IPA highlighted

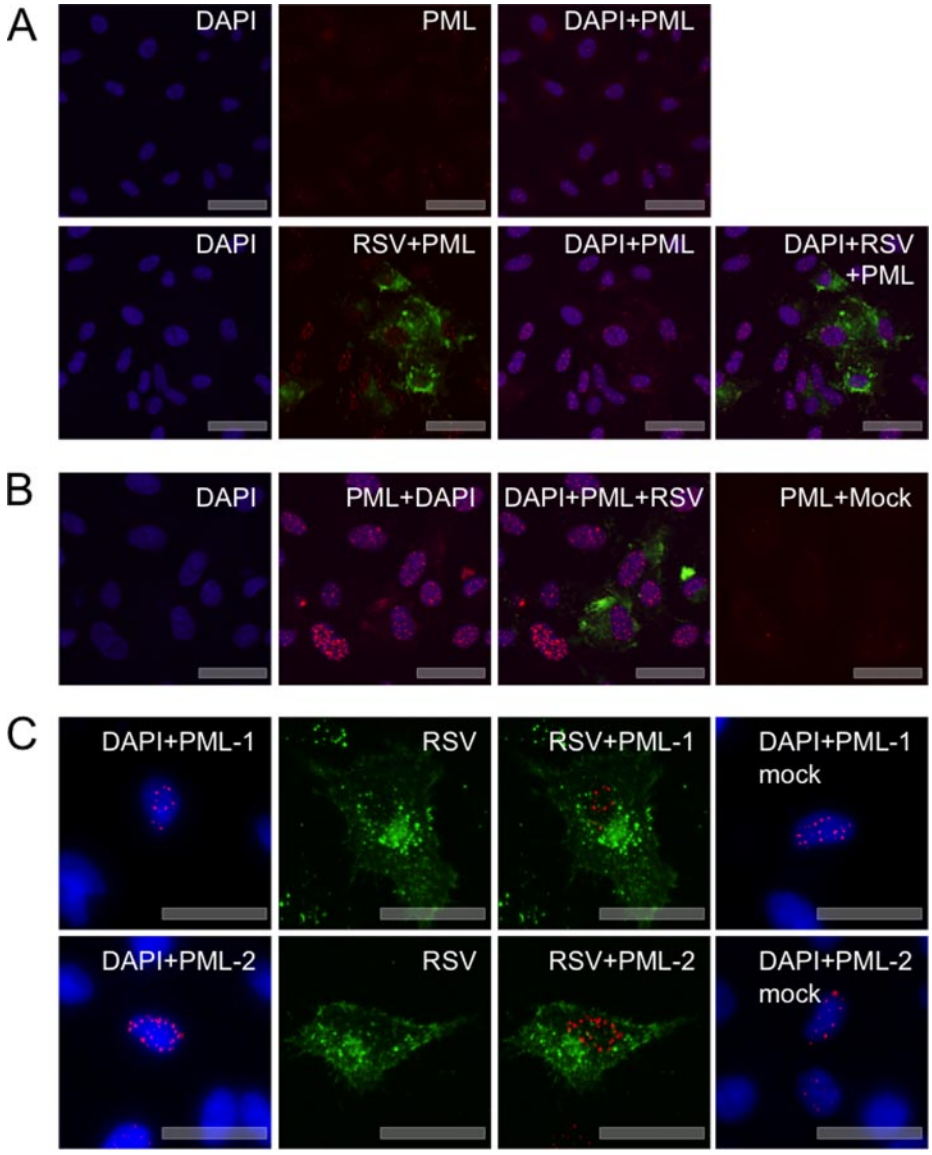

FIG. 12. **Indirect immunofluorescence confocal microscopy analysis of ND10s in HRSV-infected *versus* mock-infected cells at 24 h postinfection (*A*) and 36 h postinfection (*B*) is shown.** PML proteins (the major constituent of ND10s) are stained *red*, the HRSV proteins are *green*, and the DNA in nuclei is stained *blue* with DAPI. A merge image is also presented. *C*, direct immunofluorescence confocal microscopy analysis of the subcellular localization of recombinant FLAG-tagged PML isoforms PML-I and PML-II in mock- and HRSV-infected A549 cells 24 h postinfection. PML-I and PML-II proteins are *red*, the HRSV proteins are *green*, and the nuclei are stained *blue* with DAPI. *Scale bars*, 20 μm. *RSV*, respiratory syncytial virus.

proteins that were previously identified as being associated with pneumonitis, inflammation, and respiratory disease. Expansion of a quantitative proteomic analysis to *in vivo* tissue samples and the use of isobaric tags (*e.g.* iTRAQ (isobaric tags for relative and absolute quantitation)) may further the investigation of possible links between HRSV infection and diseases such as asthma.

STAT1 and ISG15 were identified as being more abundant in HRSV-infected cells when compared with mock-infected cells (Fig. 5). Both of these observations were consistent with previous observations using HRSV-infected cells and *in vivo* models (20, 45, 79). In the pathway analysis, STAT1 was linked to IFN α/β (Fig. 5). STAT1 activity is also regulated by phosphorylation, and HRSV uses distinct mechanisms to either impair STAT1 phosphorylation or increase phosphorylation of STAT1β (a STAT1 variant) to repress IFN expression (80). HRSV proteins NS1 and NS2 strongly inhibit IFN α/β by preventing the phosphorylation of the IFN regulatory factor-3 (15, 16). However, the molecular pathology of HRSV infection and the mechanisms by which it circumvents IFN are still not fully understood. Different strains of HRSV can differ in their ability to block IFN type I synthesis, and likewise, cell line choice is important in such pathway studies. Therefore, a comparison of different HRSV strains using differential isotopic labeling and different cell lines (*e.g.* macrophages) may prove useful in further characterizing HRSV infection.

Alterations in Mitochondrial Proteins and Mitochondrial Integrity—The mitochondria play a role in energy production, membrane potential regulation, proliferation and cellular metabolism, and modulating cell death pathways in response to microbial infection (81). Whether mitochondria are affected by HRSV infection has not been characterized previously. Quantitative proteomic analysis coupled to IPA identified changes in mitochondrial proteins in HRSV-infected cells. The localiza-

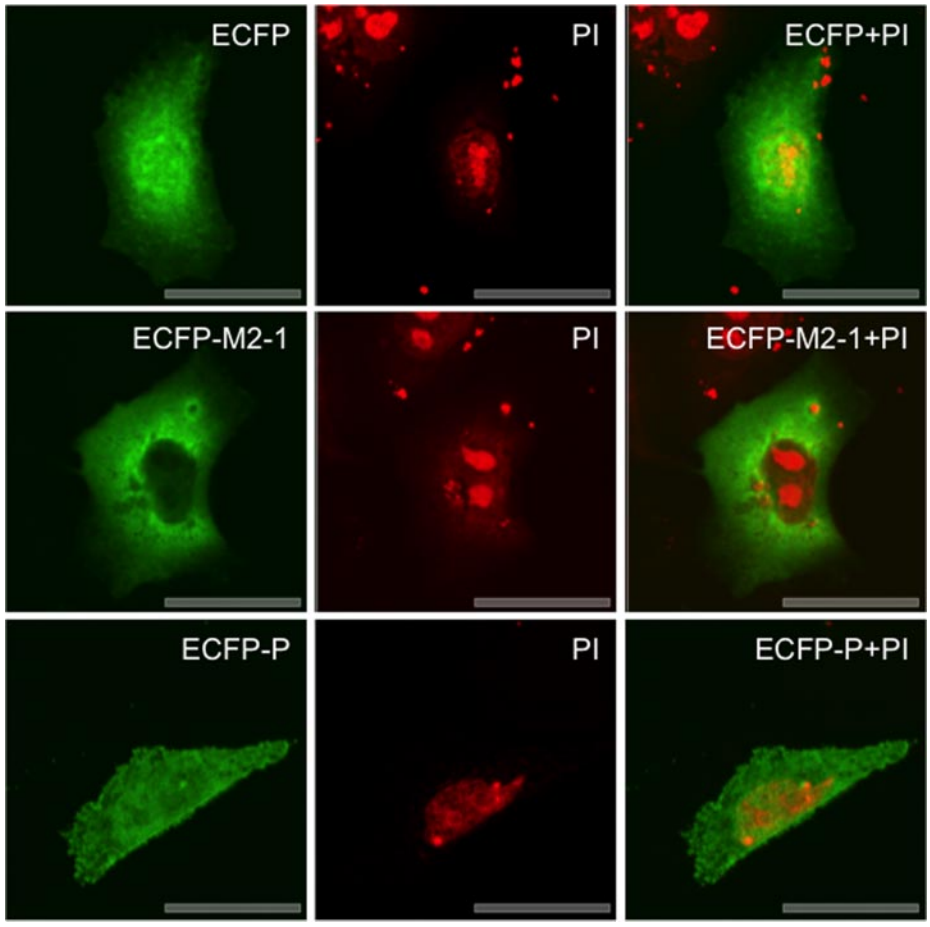

FIG. 13. **Direct immunofluorescence confocal microscopy analysis of overexpression analysis of ECFP, ECFP-M2-1, and ECFP-P in A549 cells 48 h post-transfection.** ECFP is false colored *green*, and DNA in the nuclei is stained *red* with propidium iodide (*PI*).

tion and abundance of representative mitochondrial proteins (highlighted during data analysis) were then investigated in separate experiments using indirect immunofluorescence confocal microscopy. It is of interest to note that in this analysis mitochondrial proteins were also detected in nuclear fractions. This could have been an artifact of the purification process, or it could have been due to the tubular structures that contain mitochondria and project into the nucleus (82). Certainly, the indirect immunofluorescence confocal analysis of Tom20 distribution in HRSV-infected cells reflected the latter hypothesis (supplemental Fig. 1).

Changes to mitochondrial proteins may be common in various virus-host cell interactions. For example, proteomic analysis of HCV (83) and avian influenza virus H9N2 interactions with the host cell (84) demonstrated an increase in the abundance of prohibitin. The latter study in particular showed an increased abundance value similar to the value observed in the current study. Many of the mitochondrial proteins with altered abundance in HRSV-infected cells were associated with mitochondrial membrane pore proteins. Validation using a live cell mitochondrial membrane permeability assay demonstrated a loss in the integrity of the pore complexes (Fig. 9).

Changes in the abundance and localization of mitochondrial proteins such as Toms (Fig. 7, *B* and *C*), VDACs (Fig. 8*A*), and PHBs (Fig. 8*B*) may be linked to a number of factors relating to the immune response, antiviral state, and viral infection. IPA defines mitochondrial dysfunction as anything (genetic or environmental) that interferes with the regulation of reactive oxygen species (ROS) causing the superoxide to overpower the antioxidant system. ROS are potent elements in the mitochondrial antimicrobial defense system, and mitochondria may participate in the innate immune response by triggering the production of ROS (81). However, as is the case in the IFN pathway, microbes may have evolved strategies to manipulate such defense mechanisms, and any alterations in mitochondrial function may affect the immune response of cells to virus infection. For example, HCV is able to block the mitochondrial antiviral signaling protein (found on the outer membrane of the mitochondria) downstream signaling pathway, which leads to the expression of IFN β, thereby enabling HCV to evade host immunity (85). Furthermore, human cytomegalovirus has been shown to perturb many cellular processes that promote the release of proapoptotic molecules such as cytochrome *c* (86).

In HRSV infection, activation of retinoic acid-inducible gene-1 (RIG-I) induces an antiviral response (87) that involves its association with the mitochondrial antiviral signaling protein, allowing the recruitment of signaling adapters to the

mitochondrial surface. Subsequent activation of the signaling complex is followed by translocation of NF-κB into the nucleus and the activation of associated genes (88). HRSV has been shown to activate cytoplasmic mitogen- and stress-related kinase 1 (MSK1) via ROS, and in turn, MSK1 mediates NF-κB activity (88). Although the molecular basis for ROS-dependent MSK1 activation is unknown, the identification of pathways that control NF-κB activation in response to HRSV infection may be useful in finding a way to attenuate the proinflammatory effects of HRSV and lung inflammation (88). Bioinformatics analysis of quantitative proteomics data may highlight different pathways that lead to NF-κB activation in HRSV-infected cells (*e.g.* Figs. 4 and 5).

Potential Disruption of Nucleocytoplasmic Trafficking and Nuclear Pore Complex Proteins—In HRSV-infected cells, several proteins associated with nucleocytoplasmic trafficking and the nuclear pore complex were identified as altered, including nup96 and nup98. This could be a common feature of RNA virus infection (89) as other negative strand RNA viruses that replicate in the cytoplasm, such as vesicular stomatitis virus, have been shown to inhibit RAN-dependent trafficking (90). Specifically, the virus-encoded matrix protein can inhibit nuclear import and export (91). This virus has been shown to target nup96 and nup98 for degradation (92), potentially to inhibit antiviral activity (93). nup98 is an IFN-induced nuclear pore complex protein with a major role in the export of mRNA. The positive strand RNA viruses poliovirus and rhinovirus are also capable of inhibiting nucleocytoplasmic trafficking (94, 95), and nup98 is degraded in rhinovirus-infected cells (96).

Deregulation of Cell Cycle—The quantitative proteomic analysis, IPA, and subsequent validation with Western blotting revealed changes in the abundance of cell cycle regulatory complexes in HRSV-infected cells. Most notably obvious was the ablation of Cdc2 and the major cyclins responsible for cell cycle progression (Fig. 11). Also of interest was the ablation of nucleolin (Fig. 11), which under normal growth conditions is highly expressed in proliferating cells (97) and is responsible for correct mitosis and controlled centrosome duplication (98, 99). The ablation of cell cycle regulatory complexes may account for the observed cell cycle arrest reported in HRSV-infected primary and A549 cells (18) and in cells infected with bovine respiratory syncytial virus (100). A number of viruses with RNA genomes whose site of RNA synthesis is the cytoplasm have been reported to interact with the cell cycle to promote cellular conditions more favorable for viral replication. These include other negative sense RNA viruses such as measles virus, which can arrest cells in the G_0 phase to prevent an antiviral response (101–103). Also, the positive sense RNA coronavirus infectious bronchitis virus arrests cells in G_2/M to increase viral protein translation and progeny virus production (104).

Disruption to Subnuclear Structures—The nucleus contains several subnuclear structures with defined functions. These structures are believed to form around hub proteins and are composed of protein-protein and protein-nucleic acid interactions (64, 105). In this study, the abundance of proteins associated with the nucleolus and ND10s were altered in HRSV-infected cells. Both the nucleolus and ND10s are dynamic structures whose proteins are in constant interchange with the nucleoplasm whose specific composition can depend on the metabolic state of the cell, and ND10s are associated with antiviral defense (63).

Both RNA and DNA viruses target the nucleolus and its structure, and the proteome can change in response to viral infection (61, 106). In this study, the quantitative proteomic analysis indicated that two of the most common and most studied nucleolar proteins, nucleolin and nucleophosmin, were ablated in HRSV-infected cells. For nucleolin, this was confirmed by Western blot analysis (Fig. 11), demonstrating the strength of the SILAC approach. Recently, it has been shown that lamin B1 interacts with nucleophosmin to maintain nucleolar structure for ribosome biogenesis (107). However, the loss of lamin B1 resulted in the breakdown of the nucleolus (107). Our analysis indicated that lamin B1 was potentially cleaved and depleted in HRSV-infected cells (Fig. 1*C*). However, the observation of degradation of lamin B was antibody-dependent (*e.g.* compare Fig. 1*C* with Fig. 11). Nucleolin was also observed to decrease in human metapneumovirus-infected cells using 2DE (27).

Proteins associated with ND10s were also altered in HRSV-infected cells. ND10 constituents TAR and RAD50 were significantly decreased in abundance, but the major constituent, the PML protein, was not detected by LC-MS/MS. Because PML is an ND10 marker protein, it was used to validate the abundance and localization of ND10s in HRSV-infected cells. Western blot analysis indicated that the abundance of PML protein increased in the nucleus of HRSV-infected cells. This was confirmed by indirect immunofluorescence confocal microscopy that showed an increased number of ND10s in the nucleus of HRSV-infected cells. These results are in contrast to a previous report for A549 cells infected with HRSV A2 strain (26). However, in the current analysis, indirect immunofluorescence confocal microscopy positively identified HRSV-infected cells and showed that tagged PML-I and PML-II proteins remain in the nucleus. However, this does not preclude that certain isoforms may be more abundant in the cytoplasm of infected cells. Other negative sense RNA viruses have also been shown to interact with ND10s. For example, in rabies virus-infected cells, ND10s became larger, and the expression of rabies virus P protein led to the sequestration of PML in the cytoplasm, which resulted in an increased viral titer, presumably through the ablation of an antiviral response (108). Along with the observations described above and the contrasting results from previous studies, it is important to note that ND10s are dynamic nuclear structures whose composition is highly dependent on the metabolic state of the cell.

Identification of Virus Proteins in Nuclear and Cytoplasmic Fractions—Several virus-encoded proteins were identified in the nuclear and cytoplasmic fractions. For the nuclear fraction (supplemental Table 6), one of these could be predicted, the M protein, as this has well characterized nuclear-cytoplasmic trafficking (69, 109, 110). Overexpression analysis using fluorescently labeled M2-1 and P proteins indicated that these proteins were present in the nucleus but predominately localized to the cytoplasm (Fig. 13), and hence this could explain why they were identified in both fractions. The F protein was detected in the cytoplasmic fraction only (supplemental Table 7), which may be due to the association of this protein with the cellular membrane. Viral proteins could not be quantified in this experimental system as there were no unlabeled virus peptides of known amount in the isolated fractions with which to compare. However, the comparison of viral peptides with mammalian peptides (some of which may have similar sequences) does allow some putative observations to be made regarding the relative amounts of the identified viral proteins. Examination of the viral protein ratios in the cytoplasmic fraction (supplemental Table 7) indicated that the relative protein abundance of the identified proteins reflected their position on the genome and hence the abundance of their corresponding mRNA. This correlates with the relationship between gene position on the genome and abundance of mRNA in the Mononegavirales (111–113). This may also explain why no L protein was detected in the LC-MS/MS analysis as this is the least abundant virus protein in HRSV-infected cells. Several other HRSV-encoded proteins were not detected, including the NS-2, SH, and G proteins. This may be a function of their post-translational modifications (*e.g.* glycosylation of G protein) or indicative of protein stability and turnover inside a cell.

Conclusions—Although RNA synthesis and virus assembly occur in the cytoplasm, HRSV is known to induce nuclear responses in the cell as replication alters host gene expression. The relative changes in the abundance of cellular proteins in HRSV-infected cells observed in this study confirmed aspects of what is already known about changes in the host cell proteome, validating our novel approach and extending this information as well discovering novel interactions with defined cellular pathways. The application of LC-MS/MS coupled to SILAC has not been used previously to study negative sense RNA viruses and their interactions with the host cell, and this study is the first that gives a global overview of the host cell response to HRSV infection. This opens up new potential targets for therapeutic intervention and a deeper understanding of viral pathogenesis.

Acknowledgments—Dr. Patricia Cane at the Health Protection Agency is thanked for the provision of the HRSV A2 strain used in this study. Dr. Keith Leppard at the University of Warwick is thanked for the use of the FLAG-tagged PML constructs. Dr. Stephen Griffin, Dr. Jamel Mankouri, and Dr. Elisabetta Groppelli are thanked for advice regarding the mitochondrial transition pore assay. Dr. Stefanie Jourdan, Petra Gorny, and Sian Tanner are thanked for help with various different aspects of the study. Dr. Paul Ajuh at Dundee Cell Products Ltd. is thanked for help in interpretation and preparation of LC-MS/MS data.

* This work was supported in part by a Medical Research Council (MRC) training account Ph.D. studentship (to D. C. M.), a Wellcome Trust Ph.D. studentship (to C.-H. L.), a Biotechnology and Biological Sciences Research Council (BBSRC) doctoral training grant studentship (to E. E.), a BBSRC/Health Protection Agency Cooperative Awards in Science and Engineering studentship (to R. S.), MRC Models of Disease Grant G0801001 (to W. P. D.), and the award of a Leverhulme Trust Research Fellow (to J. A. H.).

** A Research Councils UK fellow.

‡‡ To whom correspondence should be addressed: Inst. of Molecular and Cellular Biology, Faculty of Biological Sciences, University of Leeds, Garstang Bldg., Rm. 8.58, Leeds LS2 9JT, UK. Tel.: 44-113-343-5582; Fax: 44-113-343-5638; E-mail: j.a.hiscox@leeds.ac.uk.

REFERENCES

1. Hall, C. B., Weinberg, G. A., Iwane, M. K., Blumkin, A. K., Edwards, K. M., Staat, M. A., Auinger, P., Griffin, M. R., Poehling, K. A., Erdman, D., Grijalva, C. G., Zhu, Y., and Szilagyi, P. (2009) The burden of respiratory syncytial virus infection in young children. *N. Engl. J. Med.* **360,** 588–598
2. Openshaw, P. J., Dean, G. S., and Culley, F. J. (2003) Links between respiratory syncytial virus bronchiolitis and childhood asthma: clinical and research approaches. *Pediatr. Infect. Dis. J.* **22,** S58–S64; discussion S64–S65
3. Martinez, F. D. (2003) Respiratory syncytial virus bronchiolitis and the pathogenesis of childhood asthma. *Pediatr. Infect. Dis. J.* **22,** S76–82
4. Collins, P. L., and Murphy, B. R. (2002) Respiratory syncytial virus: reverse genetics and vaccine strategies. *Virology* **296,** 204–211
5. Collins, P. L., and Graham, B. S. (2008) Viral and host factors in human respiratory syncytial virus pathogenesis. *J. Virol.* **82,** 2040–2055
6. Whelan, S. P., Barr, J. N., and Wertz, G. W. (2004) Transcription and replication of nonsegmented negative-strand RNA viruses. *Curr. Top. Microbiol. Immunol.* **283,** 61–119
7. Levine, S., Klaiber-Franco, R., and Paradiso, P. R. (1987) Demonstration that glycoprotein G is the attachment protein of respiratory syncytial virus. *J. Gen. Virol.* **68,** 2521–2524
8. Martín, D., Calder, L. J., García-Barreno, B., Skehel, J. J., and Melero, J. A. (2006) Sequence elements of the fusion peptide of human respiratory syncytial virus fusion protein required for activity. *J. Gen. Virol.* **87,** 1649–1658
9. Ghildyal, R., Ho, A., and Jans, D. A. (2006) Central role of the respiratory syncytial virus matrix protein in infection. *FEMS Microbiol. Rev.* **30,** 692–705
10. Carter, S. D., Dent, K. C., Atkins, E., Foster, T. L., Verow, M., Gorny, P., Harris, M., Hiscox, J. A., Ranson, N. A., Griffin, S., and Barr, J. N. (2010) Direct visualization of the small hydrophobic protein of human respiratory syncytial virus reveals the structural basis for membrane permeability. *FEBS Lett.* **584,** 2786–2790
11. Villanueva, N., Hardy, R., Asenjo, A., Yu, Q., and Wertz, G. (2000) The bulk of the phosphorylation of human respiratory syncytial virus phosphoprotein is not essential but modulates viral RNA transcription and replication. *J. Gen. Virol.* **81,** 129–133
12. Hardy, R. W., and Wertz, G. W. (1998) The product of the respiratory syncytial virus M2 gene ORF1 enhances readthrough of intergenic junctions during viral transcription. *J. Virol.* **72,** 520–526
13. Fearns, R., and Collins, P. L. (1999) Role of the M2-1 transcription antitermination protein of respiratory syncytial virus in sequential transcription. *J. Virol.* **73,** 5852–5864
14. Bermingham, A., and Collins, P. L. (1999) The M2-2 protein of human respiratory syncytial virus is a regulatory factor involved in the balance between RNA replication and transcription. *Proc. Natl. Acad. Sci. U.S.A.* **96,** 11259–11264
15. Bossert, B., and Conzelmann, K. K. (2002) Respiratory syncytial virus (RSV) nonstructural (NS) proteins as host range determinants: a chi-

meric bovine RSV with NS genes from human RSV is attenuated in interferon-competent bovine cells. *J. Virol.* **76,** 4287–4293
16. Bossert, B., Marozin, S., and Conzelmann, K. K. (2003) Nonstructural proteins NS1 and NS2 of bovine respiratory syncytial virus block activation of interferon regulatory factor 3. *J. Virol.* **77,** 8661–8668
17. Schlender, J., Bossert, B., Buchholz, U., and Conzelmann, K. K. (2000) Bovine respiratory syncytial virus nonstructural proteins NS1 and NS2 cooperatively antagonize alpha/beta interferon-induced antiviral response. *J. Virol.* **74,** 8234–8242
18. Gibbs, J. D., Ornoff, D. M., Igo, H. A., Zeng, J. Y., and Imani, F. (2009) Cell cycle arrest by transforming growth factor beta1 enhances replication of respiratory syncytial virus in lung epithelial cells. *J. Virol.* **83,** 12424–12431
19. Yeo, D. S., Chan, R., Brown, G., Ying, L., Sutejo, R., Aitken, J., Tan, B. H., Wenk, M. R., and Sugrue, R. J. (2009) Evidence that selective changes in the lipid composition of raft-membranes occur during respiratory syncytial virus infection. *Virology* **386,** 168–182
20. Swedan, S., Musiyenko, A., and Barik, S. (2009) Respiratory syncytial virus nonstructural proteins decrease levels of multiple members of the cellular interferon pathways. *J. Virol.* **83,** 9682–9693
21. Choudhary, S., Boldogh, S., Garofalo, R., Jamaluddin, M., and Brasier, A. R. (2005) Respiratory syncytial virus influences NF-kappaB-dependent gene expression through a novel pathway involving MAP3K14/NIK expression and nuclear complex formation with NF-kappaB2. *J. Virol.* **79,** 8948–8959
22. Thomas, K. W., Monick, M. M., Staber, J. M., Yarovinsky, T., Carter, A. B., and Hunninghake, G. W. (2002) Respiratory syncytial virus inhibits apoptosis and induces NF-kappa B activity through a phosphatidylinositol 3-kinase-dependent pathway. *J. Biol. Chem.* **277,** 492–501
23. Murawski, M. R., Bowen, G. N., Cerny, A. M., Anderson, L. J., Haynes, L. M., Tripp, R. A., Kurt-Jones, E. A., and Finberg, R. W. (2009) Respiratory syncytial virus activates innate immunity through Toll-like receptor 2. *J. Virol.* **83,** 1492–1500
24. Martínez, I., Lombardía, L., García-Barreno, B., Domínguez, O., and Melero, J. A. (2007) Distinct gene subsets are induced at different time points after human respiratory syncytial virus infection of A549 cells. *J. Gen. Virol.* **88,** 570–581
25. McGillivary, G., Mason, K. M., Jurcisek, J. A., Peeples, M. E., and Bakaletz, L. O. (2009) Respiratory syncytial virus-induced dysregulation of expression of a mucosal beta-defensin augments colonization of the upper airway by non-typeable Haemophilus influenzae. *Cell. Microbiol.* **11,** 1399–1408
26. Brasier, A. R., Spratt, H., Wu, Z., Boldogh, I., Zhang, Y., Garofalo, R. P., Casola, A., Pashmi, J., Haag, A., Luxon, B., and Kurosky, A. (2004) Nuclear heat shock response and novel nuclear domain 10 reorganization in respiratory syncytial virus-infected A549 cells identified by high-resolution two-dimensional gel electrophoresis. *J. Virol.* **78,** 11461–11476
27. van Diepen, A., Brand, H. K., Sama, I., Lambooy, L. H., van den Heuvel, L. P., van der Well, L., Huynen, M., Osterhaus, A. D., Andeweg, A. C., and Hermans, P. W. (2010) Quantitative proteome profiling of respiratory virus-infected lung epithelial cells. *J. Proteomics* **73,** 1680–1693
28. Eckardt-Michel, J., Lorek, M., Baxmann, D., Grunwald, T., Keil, G. M., and Zimmer, G. (2008) The fusion protein of respiratory syncytial virus triggers p53-dependent apoptosis. *J. Virol.* **82,** 3236–3249
29. Spann, K. M., Tran, K. C., and Collins, P. L. (2005) Effects of nonstructural proteins NS1 and NS2 of human respiratory syncytial virus on interferon regulatory factor 3, NF-kappaB, and proinflammatory cytokines. *J. Virol.* **79,** 5353–5362
30. Reimers, K., Buchholz, K., and Werchau, H. (2005) Respiratory syncytial virus M2-1 protein induces the activation of nuclear factor kappa B. *Virology* **331,** 260–268
31. Vester, D., Rapp, E., Gade, D., Genzel, Y., and Reichl, U. (2009) Quantitative analysis of cellular proteome alterations in human influenza A virus-infected mammalian cell lines. *Proteomics* **9,** 3316–3327
32. Ciotti, M., Marzano, V., Giuliani, L., Nuccetelli, M., D'Aguanno, S., Azzimonti, B., Bernardini, S., Perno, C. F., Urbani, A., Favalli, C., and Federici, G. (2009) Proteomic investigation in A549 lung cell line stably infected by HPV16E6/E7 oncogenes. *Respiration* **77,** 427–439
33. Forbus, J., Spratt, H., Wiktorowicz, J., Wu, Z., Boldogh, I., Denner, L., Kurosky, A., Brasier, R. C., Luxon, B., and Brasier, A. R. (2006) Functional analysis of the nuclear proteome of human A549 alveolar epithelial cells by HPLC-high resolution 2-D gel electrophoresis. *Proteomics* **6,** 2656–2672
34. Murphy, B. R., Prince, G. A., Lawrence, L. A., Croen, K. D., and Collins, P. L. (1990) Detection of respiratory syncytial virus (RSV) infected cells by in situ hybridization in the lungs of cotton rats immunized with formalin-inactivated virus or purified RSV F and G glycoprotein subunit vaccine and challenged with RSV. *Virus Res.* **16,** 153–162
35. McKimm-Breschkin, J. L. (2004) A simplified plaque assay for respiratory syncytial virus—direct visualization of plaques without immunostaining. *J. Virol. Methods* **120,** 113–117
36. Shevchenko, A., Wilm, M., Vorm, O., and Mann, M. (1996) Mass spectrometric sequencing of proteins silver-stained polyacrylamide gels. *Anal. Chem.* **68,** 850–858
37. Emmott, E., Rodgers, M. A., Macdonald, A., McCrory, S., Ajuh, P., and Hiscox, J. A. (2010) Quantitative proteomics using stable isotope labeling with amino acids in cell culture (SILAC) reveals changes in the cytoplasmic, nuclear and nucleolar proteomes in Vero cells infected with the coronavirus infectious bronchitis virus. *Mol. Cell. Proteomics* **9,** 1920–1936
38. Olsen, J. V., de Godoy, L. M., Li, G., Macek, B., Mortensen, P., Pesch, R., Makarov, A., Lange, O., Horning, S., and Mann, M. (2005) Parts per million mass accuracy on an Orbitrap mass spectrometer via lock mass injection into a C-trap. *Mol. Cell. Proteomics* **4,** 2010–2021
39. Cox, J., and Mann, M. (2008) MaxQuant enables high peptide identification rates, individualized p.p.b.-range mass accuracies and proteome-wide protein quantification. *Nat. Biotechnol.* **26,** 1367–1372
40. Beech, S. J., Lethbridge, K. J., Killick, N., McGlincy, N., and Leppard, K. N. (2005) Isoforms of the promyelocytic leukemia protein differ in their effects on ND10 organization. *Exp. Cell Res.* **307,** 109–117
41. Mann, M. (2006) Functional and quantitative proteomics using SILAC. *Nat. Rev. Mol. Cell Biol.* **7,** 952–958
42. Ebbert, J. O., and Limper, A. H. (2005) Respiratory syncytial virus pneumonitis in immunocompromised adults: clinical features and outcome. *Respiration* **72,** 263–269
43. Young, D. F., Didcock, L., Goodbourn, S., and Randall, R. E. (2000) Paramyxoviridae use distinct virus-specific mechanisms to circumvent the interferon response. *Virology* **269,** 383–390
44. Durbin, J. E., Johnson, T. R., Durbin, R. K., Mertz, S. E., Morotti, R. A., Peebles, R. S., and Graham, B. S. (2002) The role of IFN in respiratory syncytial virus pathogenesis. *J. Immunol.* **168,** 2944–2952
45. Moore, E. C., Barber, J., and Tripp, R. A. (2008) Respiratory syncytial virus (RSV) attachment and nonstructural proteins modify the type I interferon response associated with suppressor of cytokine signaling (SOCS) proteins and IFN-stimulated gene-15 (ISG15). *Virol. J.* **5,** 116
46. Johnson, T. R., Mertz, S. E., Gitiban, N., Hammond, S., Legallo, R., Durbin, R. K., and Durbin, J. E. (2005) Role for innate IFNs in determining respiratory syncytial virus immunopathology. *J. Immunol.* **174,** 7234–7241
47. Bose, S., Kar, N., Maitra, R., DiDonato, J. A., and Banerjee, A. K. (2003) Temporal activation of NF-kappaB regulates an interferon-independent innate antiviral response against cytoplasmic RNA viruses. *Proc. Natl. Acad. Sci. U.S.A.* **100,** 10890–10895
48. Merkwirth, C., Dargazanli, S., Tatsuta, T., Geimer, S., Löwer, B., Wunderlich, F. T., von Kleist-Retzow, J. C., Waisman, A., Westermann, B., and Langer, T. (2008) Prohibitins control cell proliferation and apoptosis by regulating OPA1-dependent cristae morphogenesis in mitochondria. *Genes Dev.* **22,** 476–488
49. Osman, C., Merkwirth, C., and Langer, T. (2009) Prohibitins and the functional compartmentalization of mitochondrial membranes. *J. Cell Sci.* **122,** 3823–3830
50. Krull, S., Thyberg, J., Björkroth, B., Rackwitz, H. R., and Cordes, V. C. (2004) Nucleoporins as components of the nuclear pore complex core structure and Tpr as the architectural element of the nuclear basket. *Mol. Biol. Cell* **15,** 4261–4277
51. Boer, J. M., van Deursen, J. M., Croes, H. J., Fransen, J. A., and Grosveld, G. C. (1997) The nucleoporin CAN/Nup214 binds to both the cytoplasmic and the nucleoplasmic sides of the nuclear pore complex in overexpressing cells. *Exp. Cell Res.* **232,** 182–185
52. Miller, B. R., Powers, M., Park, M., Fischer, W., and Forbes, D. J. (2000) Identification of a new vertebrate nucleoporin, Nup188, with the use of

a novel organelle trap assay. *Mol. Biol. Cell* **11,** 3381–3396
53. Melcák, I., Hoelz, A., and Blobel, G. (2007) Structure of Nup58/45 suggests flexible nuclear pore diameter by intermolecular sliding. *Science* **315,** 1729–1732
54. Hawryluk-Gara, L. A., Platani, M., Santarella, R., Wozniak, R. W., and Mattaj, I. W. (2008) Nup53 is required for nuclear envelope and nuclear pore complex assembly. *Mol. Biol. Cell* **19,** 1753–1762
55. Hawryluk-Gara, L. A., Shibuya, E. K., and Wozniak, R. W. (2005) Vertebrate Nup53 interacts with the nuclear lamina and is required for the assembly of a Nup93-containing complex. *Mol. Biol. Cell* **16,** 2382–2394
56. Boehmer, T., Jeudy, S., Berke, I. C., and Schwartz, T. U. (2008) Structural and functional studies of Nup107/Nup133 interaction and its implications for the architecture of the nuclear pore complex. *Mol. Cell* **30,** 721–731
57. Franz, C., Askjaer, P., Antonin, W., Iglesias, C. L., Haselmann, U., Schelder, M., de Marco, A., Wilm, M., Antony, C., and Mattaj, I. W. (2005) Nup155 regulates nuclear envelope and nuclear pore complex formation in nematodes and vertebrates. *EMBO J.* **24,** 3519–3531
58. Boehmer, T., Enninga, J., Dales, S., Blobel, G., and Zhong, H. (2003) Depletion of a single nucleoporin, Nup107, prevents the assembly of a subset of nucleoporins into the nuclear pore complex. *Proc. Natl. Acad. Sci. U.S.A.* **100,** 981–985
59. Aleem, E., Kiyokawa, H., and Kaldis, P. (2005) Cdc2-cyclin E complexes regulate the G1/S phase transition. *Nat. Cell Biol.* **7,** 831–836
60. Kaldis, P., and Aleem, E. (2005) Cell cycle sibling rivalry: Cdc2 vs. Cdk2. *Cell Cycle* **4,** 1491–1494
61. Hiscox, J. A. (2007) RNA viruses: hijacking the dynamic nucleolus. *Nat. Rev. Microbiol.* **5,** 119–127
62. Tavalai, N., and Stamminger, T. (2008) New insights into the role of the subnuclear structure ND10 for viral infection. *Biochim. Biophys. Acta* **1783,** 2207–2221
63. Everett, R. D., and Chelbi-Alix, M. K. (2007) PML and PML nuclear bodies: implications in antiviral defence. *Biochimie* **89,** 819–830
64. Emmott, E., and Hiscox, J. A. (2009) Nucleolar targetting: the hub of the matter. *EMBO Rep.* **10,** 231–238
65. Zimber, A., Nguyen, Q. D., and Gespach, C. (2004) Nuclear bodies and compartments: functional roles and cellular signalling in health and disease. *Cell. Signal*. **16,** 1085–1104
66. Borden, K. L. (2002) Pondering the promyelocytic leukemia protein (PML) puzzle: possible functions for PML nuclear bodies. *Mol. Cell. Biol.* **22,** 5259–5269
67. Ghildyal, R., Ho, A., Dias, M., Soegiyono, L., Bardin, P. G., Tran, K. C., Teng, M. N., and Jans, D. A. (2009) The respiratory syncytial virus matrix protein possesses a Crm1-mediated nuclear export mechanism. *J. Virol.* **83,** 5353–5362
68. Ghildyal, R., Ho, A., Wagstaff, K. M., Dias, M. M., Barton, C. L., Jans, P., Bardin, P., and Jans, D. A. (2005) Nuclear import of the respiratory syncytial virus matrix protein is mediated by importin beta1 independent of importin alpha. *Biochemistry* **44,** 12887–12895
69. Ghildyal, R., Baulch-Brown, C., Mills, J., and Meanger, J. (2003) The matrix protein of Human respiratory syncytial virus localises to the nucleus of infected cells and inhibits transcription. *Arch. Virol.* **148,** 1419–1429
70. Ong, S. E., Blagoev, B., Kratchmarova, I., Kristensen, D. B., Steen, H., Pandey, A., and Mann, M. (2002) Stable isotope labeling by amino acids in cell culture, SILAC, as a simple and accurate approach to expression proteomics. *Mol. Cell. Proteomics* **1,** 376–386
71. Mannová, P., Fang, R., Wang, H., Deng, B., McIntosh, M. W., Hanash, S. M., and Beretta, L. (2006) Modification of host lipid raft proteome upon hepatitis C virus replication. *Mol. Cell. Proteomics* **5,** 2319–2325
72. Skiba, M., Mettenleiter, T. C., and Karger, A. (2008) Quantitative whole-cell proteome analysis of pseudorabies virus-infected cells. *J. Virol.* **82,** 9689–9699
73. Lam, Y. W., Evans, V. C., Heesom, K. J., Lamond, A. I., and Matthews, D. A. (2010) Proteomics analysis of the nucleolus in adenovirus-infected cells. *Mol. Cell. Proteomics* **9,** 117–130
74. Emmott, E., Smith, C., Emmett, S. R., Dove, B. K., and Hiscox, J. A. (2010) Elucidation of the avian nucleolar proteome by quantitative proteomics using SILAC and alteration in the coronavirus infectious bronchitis virus infected cells. *Proteomics* **10,** 3558–3562
75. Lukacs, N. W., Moore, M. L., Rudd, B. D., Berlin, A. A., Collins, R. D., Olson, S. J., Ho, S. B., and Peebles, R. S., Jr. (2006) Differential immune responses and pulmonary pathophysiology are induced by two different strains of respiratory syncytial virus. *Am. J. Pathol.* **169,** 977–986
76. Smith, B. T. (1977) Cell line A549: a model system for the study of alveolar type II cell function. *Am. Rev. Respir. Dis.* **115,** 285–293
77. Chan, E. Y., Qian, W. J., Diamond, D. L., Liu, T., Gritsenko, M. A., Monroe, M. E., Camp, D. G., 2nd, Smith, R. D., and Katze, M. G. (2007) Quantitative analysis of human immunodeficiency virus type 1-infected CD4+ cell proteome: dysregulated cell cycle progression and nuclear transport coincide with robust virus production. *J. Virol.* **81,** 7571–7583
78. Zheng, X., Hong, L., Shi, L., Guo, J., Sun, Z., and Zhou, J. (2008) Proteomics analysis of host cells infected with infectious bursal disease virus. *Mol. Cell. Proteomics* **7,** 612–625
79. Hashimoto, K., Durbin, J. E., Zhou, W., Collins, R. D., Ho, S. B., Kolls, J. K., Dubin, P. J., Sheller, J. R., Goleniewska, K., O'Neal, J. F., Olson, S. J., Mitchell, D., Graham, B. S., and Peebles, R. S., Jr. (2005) Respiratory syncytial virus infection in the absence of STAT 1 results in airway dysfunction, airway mucus, and augmented IL-17 levels. *J. Allergy Clin. Immunol.* **116,** 550–557
80. Liu, T., Castro, S., Brasier, A. R., Jamaluddin, M., Garofalo, R. P., and Casola, A. (2004) Reactive oxygen species mediate virus-induced STAT activation: role of tyrosine phosphatases. *J. Biol. Chem.* **279,** 2461–2469
81. Arnoult, D., Carneiro, L., Tattoli, I., and Girardin, S. E. (2009) The role of mitochondria in cellular defense against microbial infection. *Semin. Immunol.* **21,** 223–232
82. Lui, P. P., Chan, F. L., Suen, Y. K., Kwok, T. T., and Kong, S. K. (2003) The nucleus of HeLa cells contains tubular structures for Ca2+ signaling with the involvement of mitochondria. *Biochem. Biophys. Res. Commun.* **308,** 826–833
83. Tsutsumi, T., Matsuda, M., Aizaki, H., Moriya, K., Miyoshi, H., Fujie, H., Shintani, Y., Yotsuyanagi, H., Miyamura, T., Suzuki, T., and Koike, K. (2009) Proteomics analysis of mitochondrial proteins reveals overexpression of a mitochondrial protein chaperon, prohibitin, in cells expressing hepatitis C virus core protein. *Hepatology* **50,** 378–386
84. Liu, N., Song, W., Wang, P., Lee, K., Chan, W., Chen, H., and Cai, Z. (2008) Proteomics analysis of differential expression of cellular proteins in response to avian H9N2 virus infection in human cells. *Proteomics* **8,** 1851–1858
85. Piccoli, C., Scrima, R., D'Aprile, A., Ripoli, M., Lecce, L., Boffoli, D., and Capitanio, N. (2006) Mitochondrial dysfunction in hepatitis C virus infection. *Biochim. Biophys. Acta* **1757,** 1429–1437
86. Reeves, M. B., Davies, A. A., McSharry, B. P., Wilkinson, G. W., and Sinclair, J. H. (2007) Complex I binding by virally encoded RNA regulates mitochondria-induced cell death. *Science* **316,** 1345–1348
87. Liu, P., Jamaluddin, M., Li, K., Garofalo, R. P., Casola, A., and Brasier, A. R. (2007) Retinoic acid-insoluble gene I mediates early antiviral response and Toll-like receptor 3 expression in respiratory syncytial virus-infected airway epithelial cells. *J. Virol.* **81,** 1401–1411
88. Jamaluddin, M., Tian, B., Boldogh, I., Garofalo, R. P., and Brasier, A. R. (2009) Respiratory syncytial virus infection induces a reactive oxygen species-MSK1-phospho-Ser-276 RelA pathway required for cytokine expression. *J. Virol.* **83,** 10605–10615
89. Gustin, K. E. (2003) Inhibition of nucleo-cytoplasmic trafficking by RNA viruses: targeting the nuclear pore complex. *Virus Res.* **95,** 35–44
90. Her, L. S., Lund, E., and Dahlberg, J. E. (1997) Inhibition of Ran guanosine triphosphatase-dependent nuclear transport by the matrix protein of vesicular stomatitis virus. *Science* **276,** 1845–1848
91. Petersen, J. M., Her, L. S., and Dahlberg, J. E. (2001) Multiple vesiculoviral matrix proteins inhibit both nuclear export and import. *Proc. Natl. Acad. Sci. U.S.A.* **98,** 8590–8595
92. von Kobbe, C., van Deursen, J. M., Rodrigues, J. P., Sitterlin, D., Bachi, A., Wu, X., Wilm, M., Carmo-Fonseca, M., and Izaurralde, E. (2000) Vesicular stomatitis virus matrix protein inhibits host cell gene expression by targeting the nucleoporin Nup98. *Mol. Cell* **6,** 1243–1252
93. Enninga, J., Levy, D. E., Blobel, G., and Fontoura, B. M. (2002) Role of nucleoporin induction in releasing an mRNA nuclear export block. *Science* **295,** 1523–1525
94. Gustin, K. E., and Sarnow, P. (2001) Effects of poliovirus infection on nucleo-cytoplasmic trafficking and nuclear pore complex composition. *EMBO J.* **20,** 240–249

95. Gustin, K. E., and Sarnow, P. (2002) Inhibition of nuclear import and alteration of nuclear pore complex composition by rhinovirus. *J. Virol.* **76,** 8787–8796
96. Park, N., Katikaneni, P., Skern, T., and Gustin, K. E. (2008) Differential targeting of nuclear pore complex proteins in poliovirus-infected cells. *J. Virol.* **82,** 1647–1655
97. Bicknell, K., Brooks, G., Kaiser, P., Chen, H., Dove, B. K., and Hiscox, J. A. (2005) Nucleolin is regulated both at the level of transcription and translation. *Biochem. Biophys. Res. Commun.* **332,** 817–822
98. Ma, N., Matsunaga, S., Takata, H., Ono-Maniwa, R., Uchiyama, S., and Fukui, K. (2007) Nucleolin functions in nucleolus formation and chromosome congression. *J. Cell Sci.* **120,** 2091–2105
99. Srivastava, M., and Pollard, H. B. (1999) Molecular dissection of nucleolin's role in growth and cell proliferation: new insights. *FASEB J.* **13,** 1911–1922
100. Schlender, J., Walliser, G., Fricke, J., and Conzelmann, K. K. (2002) Respiratory syncytial virus fusion protein mediates inhibition of mitogen-induced T-cell proliferation by contact. *J. Virol.* **76,** 1163–1170
101. Schnorr, J. J., Seufert, M., Schlender, J., Borst, J., Johnston, I. C., ter Meulen, V., and Schneider-Schaulies, S. (1997) Cell cycle arrest rather than apoptosis is associated with measles virus contact-mediated immunosuppression in vitro. *J. Gen. Virol.* **78,** 3217–3226
102. Niewiesk, S., Ohnimus, H., Schnorr, J. J., Götzelmann, M., Schneider-Schaulies, S., Jassoy, C., and ter Meulen, V. (1999) Measles virus-induced immunosuppression in cotton rats is associated with cell cycle retardation in uninfected lymphocytes. *J. Gen. Virol.* **80,** 2023–2029
103. Naniche, D., Reed, S. I., and Oldstone, M. B. A. (1999) Cell cycle arrest during measles virus infection: a G_0-like block leads to suppression of retinoblastoma protein expression. *J. Virol.* **73,** 1894–1901
104. Dove, B., Brooks, G., Bicknell, K., Wurm, T., and Hiscox, J. A. (2006) Cell cycle perturbations induced by infection with the coronavirus infectious bronchitis virus and their effect on virus replication. *J. Virol.* **80,** 4147–4156
105. Leppard, K. N., Emmott, E., Cortese, M. S., and Rich, T. (2009) Adenovirus type 5 E4 Orf3 protein targets promyelocytic leukaemia (PML) protein nuclear domains for disruption via a sequence in PML isoform II that is predicted as a protein interaction site by bioinformatic analysis. *J. Gen. Virol.* **90,** 95–104
106. Greco, A. (2009) Involvement of the nucleolus in replication of human viruses. *Rev. Med. Virol.* **19,** 201–214
107. Martin, C., Chen, S., Maya-Mendoza, A., Lovric, J., Sims, P. F., and Jackson, D. A. (2009) Lamin B1 maintains the functional plasticity of nucleoli. *J. Cell Sci.* **122,** 1551–1562
108. Blondel, D., Regad, T., Poisson, N., Pavie, B., Harper, F., Pandolfi, P. P., De Thé, H., and Chelbi-Alix, M. K. (2002) Rabies virus P and small P products interact directly with PML and reorganize PML nuclear bodies. *Oncogene* **21,** 7957–7970
109. Petersen, J. M., Her, L. S., Varvel, V., Lund, E., and Dahlberg, J. E. (2000) The matrix protein of vesicular stomatitis virus inhibits nucleocytoplasmic transport when it is in the nucleus and associated with nuclear pore complexes. *Mol. Cell. Biol.* **20,** 8590–8601
110. Glodowski, D. R., Petersen, J. M., and Dahlberg, J. E. (2002) Complex nuclear localization signals in the matrix protein of vesicular stomatitis virus. *J. Biol. Chem.* **277,** 46864–46870
111. Cowton, V. M., McGivern, D. R., and Fearns, R. (2006) Unravelling the complexities of respiratory syncytial virus RNA synthesis. *J. Gen. Virol.* **87,** 1805–1821
112. Krempl, C., Murphy, B. R., and Collins, P. L. (2002) Recombinant respiratory syncytial virus with the G and F genes shifted to the promoter-proximal positions. *J. Virol.* **76,** 11931–11942
113. Wertz, G. W., Perepelitsa, V. P., and Ball, L. A. (1998) Gene rearrangement attenuates expression and lethality of a nonsegmented negative strand RNA virus. *Proc. Natl. Acad. Sci. U.S.A.* **95,** 3501–3506